Geomorphology 463 (2024) 109347

Contents lists available at ScienceDirect

Geomorphology

journal homepage: www.journals.elsevier.com/geomorphology

Drainage evolution in porous carbonate terrain in semi-arid environments: The role of tectonics and climatic change – The case study of the Boukadir carbonate platform, Algeria

Meriem L. Moulana [a,b,*], Marthe Lefevre [a,c], Aurélia Hubert-Ferrari [a]

[a] Department of Geography, University of Liege, Clos Mercator 3, 4000 Liege, Belgium
[b] Underground risk unit, Institut Scientifique de Service Public (ISSeP), 4000 Liège, Belgium
[c] Seismology-Gravimetry department, Royal Observatory of Belgium, Bruxelles, Belgium

ARTICLE INFO

Keywords:
Tectonic deformation
Longitudinal profiles
Karstic platform
Differential compaction
Tilt
Calcrete
Boukadir

ABSTRACT

Porous carbonate terrains are widespread around the Mediterranean area and form non classical karstic landscapes. The related diffuse infiltration is expected to impede karstification and the establishment of dense drainage networks. In such terrain, the effect of tectonics and climate on drainage development and evolution remains poorly understood. To address this issue, we focus on a semi-arid area with a tuffaceous Messinian carbonate platform characterized by a well-established dendritic network in an active tectonic context. The platform is situated in the Chélif Basin in Algeria, affected by transpressive deformation in relation to the Africa-Eurasia collision. We combine geomorphological observations with drainage morphometric analyses using satellite images and DEM. The drainage network analysis reveals varying tectonic deformation and morphological anomalies resulting from instability in the drainage systems, expressed through (1) variable platform tilt and (2) the presence of knickpoints and convexities in river profiles. These anomalies are particularly pronounced in the west, where knickpoints are more numerous, and incisions deeper. We relate the origin of the tilt to the differential marl compaction and remobilization, and in the area with the highest tilt a recent propagation of the Boukadir thrust underneath the platform might also play a role. Finally, we propose a general model of drainage evolution which highlights the importance of weathering in the Maghreb area transforming the porous media in an indurated carbonate or calcrete.

1. Introduction

Highly porous carbonate terrains like chalks are a lithology with unique characteristics. They present very low hydraulic conductivities related to the small pore diameters that do not permit efficient flow (Vázquez et al., 2016; Gaillard et al., 2018, 2023), leading to a limited cave development and subtle surface karst features. That is why the karstic characteristic of these terrains has long been debated and speculated (Reeve, 2021). Nevertheless, several authors such as Rodet (1991), Farrant et al. (2023) and Ballesteros et al. (2023) have shown that in Cretaceous chalks in France and the UK, the dissolution still plays an important role and is associated with the development of karstic voids and conduits, forming extensive, but isolated, conduit networks. However, drainage establishment and evolution on similar porous carbonate terrains in semi-arid regions has never been assessed.

Here, we focus on a particular carbonate system composed of a highly porous media similar to chalks, the Boukadir Messinian platform, which is in a semi-arid environment in Algeria, the Boukadir platform (Fig. 1). This type of terrain is widespread around the Mediterranean Sea, in association with large marginal seas present before the Messinian Salinity Crisis (MSC: 5.97–5.33 Ma) and is usually deformed due to the progressive closure of the Mediterranean Sea (Krijgsman et al., 2018). The studied site is an ideal landscape evolution laboratory in a semi-arid setting for several reasons. First, these tuffaceous carbonates are karstified as evidenced by a large collapse sinkhole that occurred in June 1988, as well as the presence of caves and shelter caves. A deep karstification due to the MSC has also been evidenced by Moulana et al. (2022). Second, it features a dense dendritic network that is unusual in karstified formations, where infiltration is greatly enhanced by karstic voids resulting from dissolution. The dendritic drainage network

* Corresponding author at: Department of Geography, University of Liege, Clos Mercator 3, 4000 Liege, Belgium.
E-mail address: ml.moulana@uliege.be (M.L. Moulana).

https://doi.org/10.1016/j.geomorph.2024.109347
Received 1 December 2023; Received in revised form 16 July 2024; Accepted 16 July 2024
Available online 21 July 2024

suggests a landscape dominated by surface runoff. Third, the platform is located in the Maghreb region and has sustained a significant and relatively simple deformation history since its deposition compared to most chalk terrains that are less deformed. In the Maghreb region, during the last ~5 Ma, stresses have been controlled by the oblique convergence between Eurasia and Africa, and deformation is characterized by strike-slip faults and compressive structures (Meghraoui, 1982). The deformation pattern around the study area is already well studied, because it was the locus of the largest earthquake in the entire southern Mediterranean region, the 1980 El Asnam earthquake of magnitude 7.3 Mw (Ouyed et al., 1981). Finally, the platform is in a semi-arid area marked by significant changes in precipitation between rainy and inter-rainy periods and intermittent precipitations over the year leading to non-permanent streams. This context is particular and relatively different from the one in northern Europe, where many studies have been carried out on porous karst terrains, in a Quaternary climatic context with an alternation of periglacial and temperate conditions during respectively glacial and interglacial periods. This area is thus an ideal place to gain a better understanding of the evolution of drainage networks in a semi-arid context on porous carbonate landscapes in an active tectonic setting.

Here we seek to obtain a large-scale landform evolution model in direct link with incision, drainage evolution, climate and tectonics (Burbank and Anderson, 2001). For that purpose, we use an integrated morphological and morphometric approach. The morphological approach focuses on the analysis of high resolution Google Earth imagery and 12 m DEM. The morphometric approach is based on the present-day accepted model that drainage evolution occurs in accordance with the stream power incision model, as established by Howard and Kerby (1983). Stream power law has mostly been used to model bedrock river incision in response to base level changes due to climate, eustasy or tectonics (e.g. Kirby and Whipple, 2012; Kirby et al., 2003; Wobus et al., 2006). This law is questionable in fluviokarstic environments, where surface discharge does not systematically scale with drainage area, because of the competition between surface and groundwater flows and the exchanges between the two systems through sinking streams and resurgent groundwater. Nevertheless, Anthony and Granger (2007) have shown that the stream power law can be used to model knickpoint migration in fluviokarst systems. These approaches are particularly suitable in regions where climate and rock-type are uniform and allowed to unravel debated active tectonic issues (Snyder et al., 2000; Kirby et al., 2003; Wobus et al., 2006; Pérez-Peña et al., 2009; Gallen et al., 2013; Pavano, 2013; Pavano et al., 2016). The obtained landscape evolution model will allow us to create a conceptual framework for drainage development in porous carbonate terrain affected by climatic changes and tectonics.

2. Setting

2.1. Geology and geomorphology

This study focuses on the Messinian carbonated marginal platform of Boukadir, which is underlain by Tortono-Messinian blue marls (Fig. 2). North of the studied area, in the Chélif basin, the Tortono-Messinian blue marls are overlain by a gypsum formation up to 400 m thick and younger terrigenous sediments (Perrodon, 1957; Belkebir et al., 1996; Rouchy et al., 2007).

The studied carbonates are composed of two carbonate units (Neurdin-Trescartes, 1992; Moulana et al., 2021): (1) the upper compact and homogeneous unit is ~80 m thick, which is called Lithothamnium

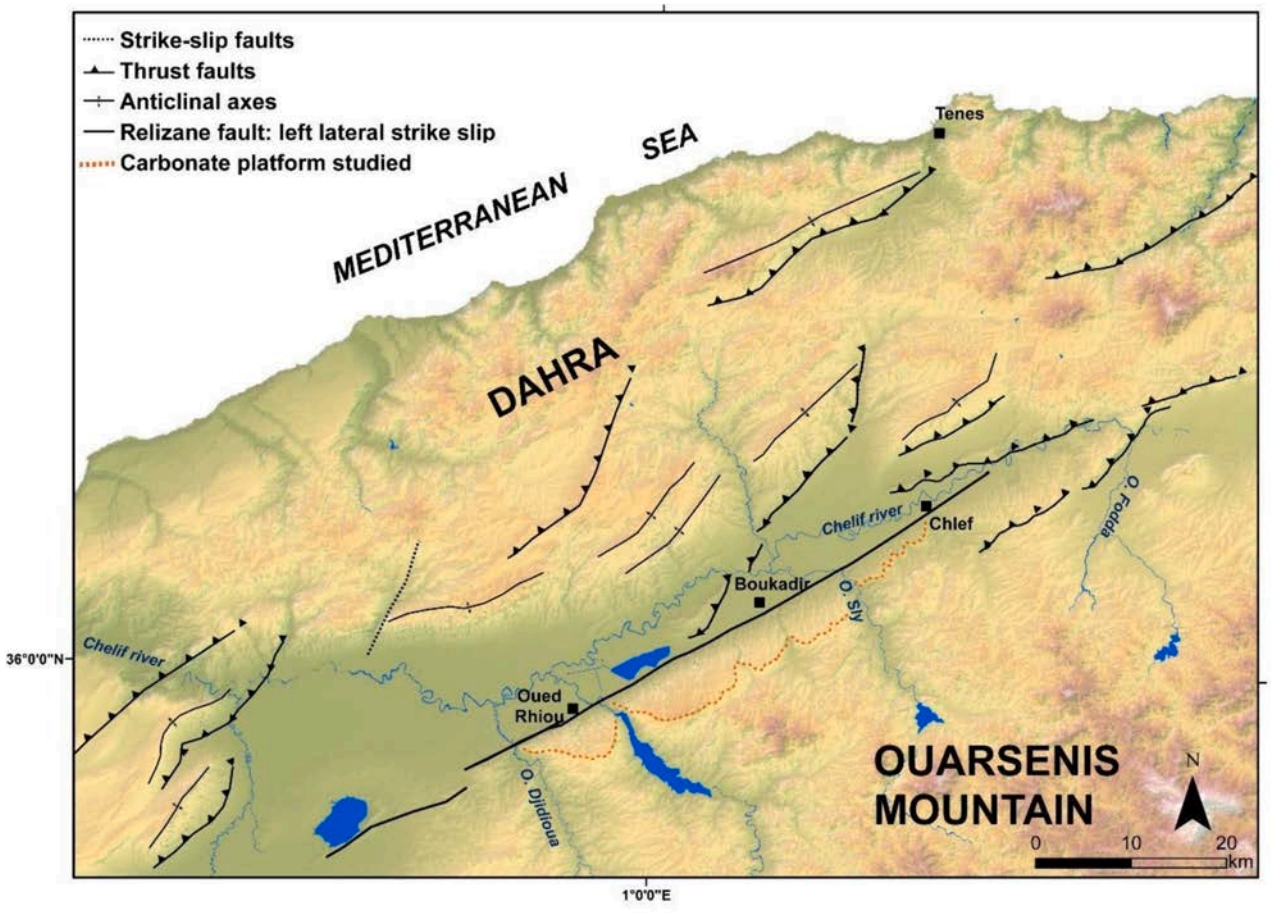

Fig. 1. Tectonic setting map of the Chélif Basin with relief from SRTM and fault mapped since Meghraoui et al. (1986).

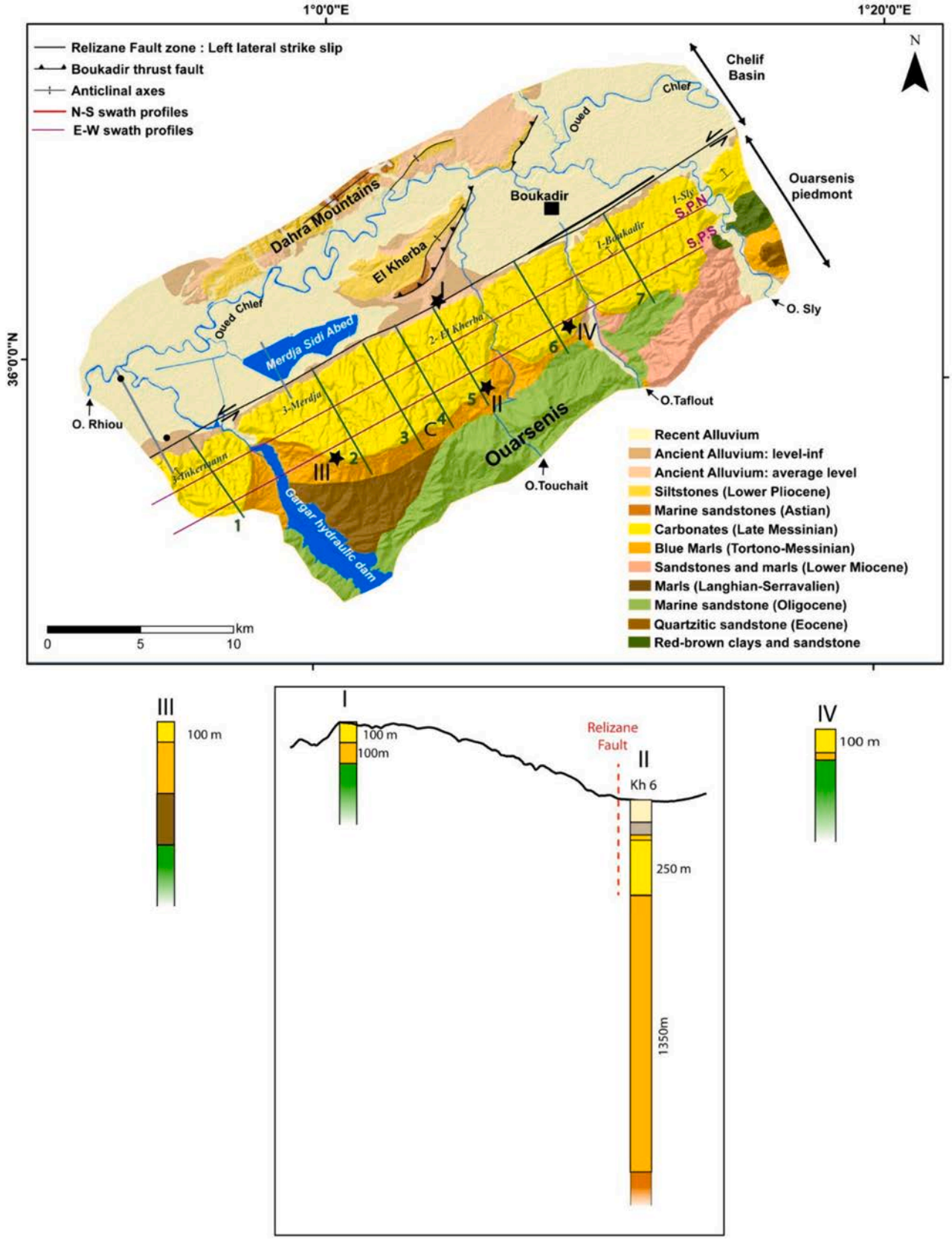

Fig. 2. Up. Geological map of the study area modified from geological map N°105 CHARON at 1/50,000 (Brives and Ferrand, 1912) with swath profile locations. NS swath profiles are represented in the green line and EW swath profiles are represented in the purple line. Spatial reference: WGS_1984_UTM_Zone_31N. **Bottom.** Stratigraphic log showing the thickness of the blue marl below the carbonate platform.

carbonates and (2) the lower less resistant unit is ~70 m thick and corresponds to bioclastic carbonates (Moulana et al., 2021). Both units are mostly composed of carbonates with very minor (<5 %) terrigenous content.

The upper Lithothamnium carbonated unit has a low dip, a high porosity (tuffaceous facies) and low permeability. It is thus similar to Cretaceous Chalk. The lower bioclastic unit is composed of well-marked banks with different bioclastic components and matrix, so it shows strong stratigraphic discontinuities. This unit can locally show clinoforms with ~35° dips (Fig. 3).

At the surface, the studied Lithothamnium tuffaceous carbonates form a hardened carbonate cover called a calcrete (Moulana et al., 2022). Calcrete formation is typical of the Maghreb region and is due to weathering in relation with its semi-arid climate (Horta, 1980). This calcrete layer limits infiltration and implies the existence of significant recurrent surface flows and concentrated fluxes along the platform main dip direction (Moulana et al., 2021, 2022).

Like other carbonate margins of the Mediterranean, the studied platform bears the imprint of the Messinian Salinity Crisis (5.97–5.33 Ma), during which it emerged and was deeply incised. This Messinian imprint is attested by deep river incisions in the carbonates presently buried by sediments.

2.2. Karstic setting

The area presents several karstic features, in particular along the southern margin of the Chélif basin a deep paleokarst, inferred to be related to the low base-level during the Messinian Salinity Crisis, has been evidenced (Moulana et al., 2022). A notable example of this ~100 m deep paleokarst is the large covered-collapse sinkhole that occurred in 1988 near Boukadir.

In the carbonate massif, there are few documented caves, their limited development has been attributed to the high porosity of the carbonates resembling chalk (Moulana et al., 2022). The two largest caves developed in the lower bioclastic unit along stratigraphic/lithologic discontinuities that formed flow conduits. These caves are presently located above the adjacent river beds due to the ongoing river incision in the carbonate terrain. At the surface, small dissolution holes, an extensive network of fissures and piping is present (Moulana et al., 2022), which enables groundwater flow. Along the valley slopes, numerous shelter caves of complex origin were documented and put in relation with calcrete formation, river incision and the endokarst (Moulana et al., 2022).

Karst development depends on rainfall. In the study area, the current semi-arid climate is characterized by precipitation of around 350 mm/year (Bettahar, 2012), easily limiting karstification processes and favoring calcrete formation. However, during the Quaternary, the northern African climate is characterized by strong change in aridity/humidity with the establishment of African wet periods or Green Sahara Periods (e.g. Shanahan et al., 2015; Tierney et al., 2017; Pausata et al., 2020) due to changes in the intertropical convergence zone (Burns et al., 2001; Rohling et al., 2002; Hoffmann et al., 2016). At the end of these wet periods, during the so-called catapluvial phase, increased calcite dissolution and precipitation led to the formation of calcrete in North Africa (Ek et al., 1981; Mathieu et al., 1983). Kartification thus evolved considerably in the study area during the Quaternary.

2.3. Tectonics

The study area is characterized by significant post-Messinian compressive deformation in relation with the oblique convergence between Africa and Eurasia (Meghraoui et al., 1988; Dewey et al., 1989; Mazzoli and Helman, 1994; Rosenbaum et al., 2002; Yelles-Chaouche et al., 2006). The Boukadir carbonate platform is bounded to the north since the Pliocene by the Relizane left-lateral strike-slip fault. The fault, trending N70°E, extends for around 150 km from the cities of Chlef to Relizane (Meghraoui et al., 1986) and offsets the Boukadir platform (Moulana et al., 2022). The fault is probably inactive as it is buried by Quaternary sediments. A dense network of fractures subparallel to the Relizane Fault has affected the studied carbonate platform but shows insignificant offset except locally at the back of the platform (Moulana et al., 2022). In the Chélif and Dahra areas, several thrusts have deformed the post-Messinian sediments, in particular near the studied area lies the Boukadir reverse fault, which is well visible in the topography especially at its south-western extremity where it is associated with the El Kherba anticline. Those thrusts are active, as attested by the Mw 7.3 earthquake at El Asnam in 1980 (Karnik, 1969; Dewey, 1991; Philip and Meghraoui, 1983). The extension and orientation of the Boukadir fault are similar to those of the El Asnam thrust activated in 1980 (Meghraoui, 1988). Thus, according to the Wells and Coppersmith (1994) 's relation, its seismic potential should be similar to that of the El Asnam thrust fault. The tectonic characteristics of the study area are expected to play an important role in the evolution of karstification in this platform as faults can act either like important pathways for water or hydrogeological barriers (Bense et al., 2013).

3. Material and methods

The morphometric analysis, consisting mostly in the extraction and analysis of the drainage network, focuses on the southern part of the study area, i.e., the carbonate platform. It is based on the analysis of a digital elevation model (TanDEM-X) from the DLR - DFD service with a

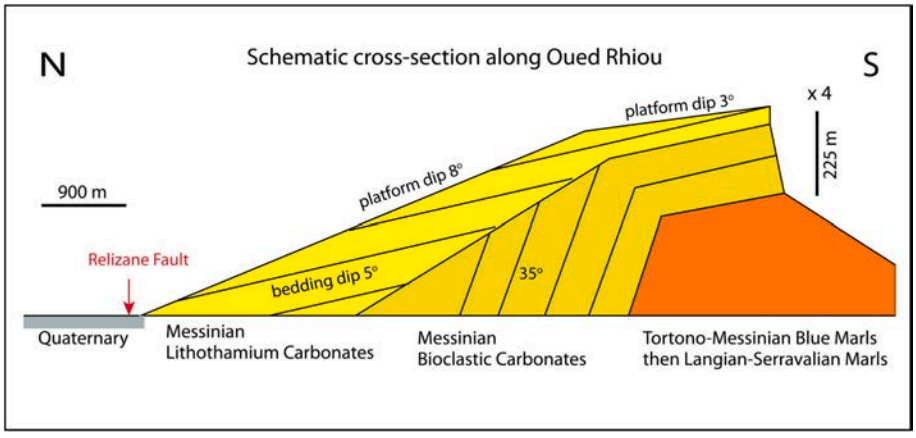

Fig. 3. Schematic cross-section along Oued Rhiou showing the two carbonate units (Lithothamnium unit and bioclastic clinoforms unit) with a vertical exaggeration of 4.

resolution of 12.5 m. The analysis has been carried out by using ArcGIS software, coupled with the TopoToolbox-MATLAB software, which allows for the calculation of k_{sn}, identification of knickpoints, and watershed dynamics through Chi (χ) analysis (Schwanghart and Scherler, 2017). The GIS-based analysis is completed by satellite imageries analysis, to identify specific morphologies, such as resurgences, wind gaps or shelter caves, as well as by field observations.

In a first step, general morphological parameters of the carbonate platform have been extracted from the DEM, such as slopes, swath profiles, and elevation of the karstic feature like shelter caves. Then, we focussed the analysis on the drainage network characteristics like the sinuosity index variation or, chi map analysis. Finally, we looked at the different watersheds and realised the river profile analysis.

For all the parameters describing the dynamics of a watercourse, we considered the existence of a channel for a drained area >1000 m^2, which, although low, seems appropriate for our terrain since a marked channel is discernible very high up in the catchment areas.

3.1. Swath profiles

Swath profiles oriented N-S and E-W have been carried out along the platform (Fig. 2-B). They provide an overall view of the topography of carbonate deposits, with potential changes in slope or lateral topographic variation, and have been widely used to characterize regional morphologies (D'Agostino et al., 2001; Riquelme et al., 2003; Grohmann, 2005; Molin et al., 2004, 2012; Scotti et al., 2014; Azañón et al., 2015). Seven topographic profiles were drawn using QGIS software and extracted using a Python code from the Tandem X DTM with sampling done every 14 m in a 1500 m large box, except for the two E-W profiles for which the box is 500 m large.

3.2. Longitudinal river profiles

For bedrock channels the stream-power incision model (Howard and Kerby, 1983) suggests that river profiles follow the power law relationship between local river slope S and the upstream drainage area A, as demonstrated by Hack (1957):

$$S = k_s A^{-\theta} \quad (1)$$

where θ is the concavity index and ks (L2θ) is the steepness index (Flint, 1974).

Within these profiles, it is possible to identify disturbances and disequilibrium states, such like knickpoints, that result from external perturbation like, tectonic, climate or local lithological variation (e.g. Crosby and Whipple, 2006; Wobus et al., 2006; Kirby and Whipple, 2012). Thus, in regions characterized by an homogenous lithology and uniform uplift, knickpoints can be considered as time-dependent geomorphic markers that migrates through the landscape, lowering the river profile to the new relative base level (e.g. Wegmann and Pazzaglia, 2002; Kirby et al., 2003; Wobus et al., 2006).

The value of k is strongly dependent on the concavity index, which can be impacted by small internal variations within the watershed. Therefore, to compare watersheds of varied shapes and sizes within the same region, we use the normalized slope index (S_n) by normalizing Eq. (1) with a reference concavity (θref) (Kirby and Whipple, 2012; Wobus et al., 2006).

$$S = k_{sn} A^{-\theta ref} \quad (2)$$

The reference concavity (θref) corresponds to the regional concavity observed in channels that are not perturbed by tectonic signals; they are identified through their distance-elevation and χ-elevation profiles that are regular (Wobus et al., 2006). Another selection criterion for the value of θref is that, within the same watershed, for the best value of θ, the different tributaries should have collinear χ-elevation curves (Mudd et al., 2014; Royden and Perron, 2013). The value of θref used here is 0.6511, it fits the classical range of values of 0.3 to 0.6 (Whipple, 2004; Wobus et al., 2006; Harkins et al., 2007; Kirby and Whipple, 2012; Lague, 2014). The concavity index (*θref*) is relatively insensitive to variation of uplift, climate or substrate lithology at steady-state, contrary to the steepness index (*ks*), which varies with these factors (e.g., Snyder et al., 2000; Kirby and Whipple, 2001;) as expressed by the equation:

$$Ksn = \left(\frac{U}{K}\right)^{1/n} \quad (3)$$

With U the uplift rate and K the erodibility coefficient and n a constant. An area at equilibrium will have homogenous averaged k_{sn} values by watersheds (Ouimet et al., 2009; Whittaker, 2012).

3.3. Chi profiles and map

The Chi (χ) is another geomorphological parameter used in the analysis of river longitudinal profiles to avoid calculation errors of the parameter (θ), induced by the use of slope/drainage area curves that are derived from slope data extracted from DEM, which are not always accurate (e.g. Lague et al., 2003; Mudd et al., 2014; Perron and Royden, 2013; Willett et al., 2014; Wobus et al., 2006). This parameter is also known to allow for deducing the drainage network dynamics and its evolution by following the migration of water divide lines (e.g., Willett et al., 2014). The formula for χ (Chi) is as follows:

$$\chi = \int_{x_0}^{x} \left(\frac{A_0}{A(x)}\right)^{\frac{m}{n}} dx \quad (4)$$

With A_0 being the reference drainage area and *m* and *n* are constant empirical parameters usually expressed as the m/n ratio, which is often considered as equivalent to the reference concavity index *θ*ref that describes how the river gradient evolves along the river profile (Willett et al., 2014). The χ plot of an equilibrated concave river following the stream power equation, with uniform conditions, is a straight line along which both main trunk stream and tributaries collapse. When calculating (χ), we used the value of θref calculated for the region.

Note that the relationships used to define k_{sn} and χ are established for rivers with rocky substrates, less permeable than the one expected in karstified areas, characterized by high infiltration and reduced runoff. Indeed, discharge in karstified areas is divided between surface channels and subsurface conduits, and channel and basin geometries usually differ when compared to non-karst basins. Nevertheless, in the studied area, we do not observe such variations. Moreover, the presence of a calcrete covering the entire platform reduces surface permeability and promotes runoff. In addition, Anthony and Granger in 2007 have shown that the stream power incision model can also be applied in karstified areas. We thus consider that this justifies the use of formulas (1) to (4).

4. Results

4.1. General morphology of the platform

The studied platform has a slab-like shape dipping towards the NNW, with variable thickness. Its southeast limit corresponds to an almost vertical escarpment forming the front of a cuesta. The morphological analysis of the platform allows us to evidence changes of relief, slope, and drainage from east to west and from north to south, which constrain its deformation and evolution.

A. Slope

In the slope map in Fig. 5, four slope classes were set-up: 0 to 3 %; 3 to 12 %; 12 to 21 % and > 21 %. The slope map highlights the morphology of the flat sedimentary basin (0–3 %) with the imprint of the Boukadir thrust fault forming an anticlinal. The Relizane fault is visible

as a straight NE-SW-oriented basin boundary delimiting the studied platform to the south (Fig. 5).

Regarding the carbonate platform, it forms a slab with a variable southward extension, with a maximum width of nearly 5 km, east of Rhiou River and a minimum of 2 km, east of Sly River. This slab has slope between 3 and 12 % (second class, Fig. 5) and presents steeper slopes in the valleys (>21 %), showing a strong incision and a highly dissected hydrographic network. The slopes associated with the incision of the hydrographic network are more pronounced in the central and western part of the platform, where the valleys can reach depths of >100 m, while in its eastern part, the incision does not exceed 50 m. This variation in incision is consistent with the variation of the maximum altitudes of the carbonate slab. Indeed, east of the Gargar dam along Rhiou River, the maximum altitude of the platform is about ~686 m while east of Taflout River, it is about ~381 m (Moulana et al., 2021). The carbonate slab ends abruptly to the south, with a marked slope break (>21 %) forming a cuesta.

Swath profiles performed perpendicularly to the platform provide additional information on the average slope and morphology of the platform. Most swath profiles show, in their upper part, a break in slope 2 to 2.5 km south of the Relizane fault, sub-parallel to it. This slope break, marked in red in Fig. 6, is more pronounced in the west, where it divides the platform into two parts. To the south, the NW oriented slope is about 2 to 4°, which is lower than the stratigraphic dip and to the north, the slope is about 4 to 9°, which is steeper than the dip of the carbonates (Fig. 3; Moulana et al., 2021). In the latter area, the platform shows a more significant incision, as highlighted along profiles 2. Locally, the slope in the upper part of the platform can be so low that a perched paleo-lake formed, as in the area west of the Gargar dam (profile 1, Fig. 6). This slope break is less pronounced east of Taflout River (swath profiles 6 in Fig. 6). It is assumed that the slope change has been present since the formation of the platform during the Messinian, linked to eustatic variations during its deposition. In some swath profiles such as swath profile 2 and 6 in Fig. 4, knickpoints are also highlighted. The location of these knickpoints is confirmed in the morphometric analysis that is discussed in the following paragraphs.

East-west "swath profiles" were also performed on both sides of the slope break in order to better constrain the lateral variation of the platform morphology (Fig. 7). Gradual changes in slope and platform elevation are observed except at the Rhiou River, where a topographic discontinuity suggests the occurrence of a fault. The existence of this fault with a NNO-SSE orientation was already proposed by Meghraoui (1982) and in geoelectrical profiles and magnetic mapping in the region by BURGEAP (2004).

These profiles allow us to distinguish three platform zones with homogeneous characteristics: a zone east of the Touchait River with lower and fairly homogeneous altitudes (around 400 m at the ridge level); a central zone between the Touchait and Rhiou Rivers where the maximum platform elevations are observed, and where large changes in slope and altitude are observed (Fig. 6); and finally, a zone to the west of the Rhiou River, separated from the rest of the platform by a fault, highlighted by the topographic jump on either side of the Rhiou river (Fig. 7).

These results confirm a 3D morphology of the carbonate slab characterized by an increase in slope towards the Relizane fault and a gradual decrease of the elevation from west to east, leading to a general dip of the platform towards the east-northeast.

B. Morphology of the cuesta and the top of the platform

Particular attention is paid to the morphology of the cuesta-shaped escarpment that delimits the platform to the south (Fig. 8). The top of the cuesta is formed by the upper Lithothamnium unit that is ~5–10 m thick there and gets thicker farther north (Fig. 3). Below this unit we observe the bioclastic unit, whose erosion results in large talus scree slopes. The lower part of the cuesta composed of more marly carbonates and marls has a lower dip. This dip change is well evidenced by slope map and in the swath profiles (Figs. 5 and 6). In the area behind the carbonate platform, the thickness of the Tortono-Messinian marls changes laterally, with a maximum thickness of ~500 m near the Rhiou River and their disappearance east of the Taflout River, where the carbonates rest on an older, non-purely marly substrate (Fig. 2; Perrodon, 1957).

The cuesta currently corresponds to the main water divide, mostly drained by north-flowing cataclinal (consequent) rivers reaching the Chélif Basin. At that location, valleys are wide and poorly incised (in general 100–200 m wide and 5–20 m deep). The large valleys at the cuesta seem truncated and are considered as wind gaps. Here, we use the term wind gap to refer to valleys formed by rivers and then abandoned due to a capture leading to the loss of the head of their watershed. As the

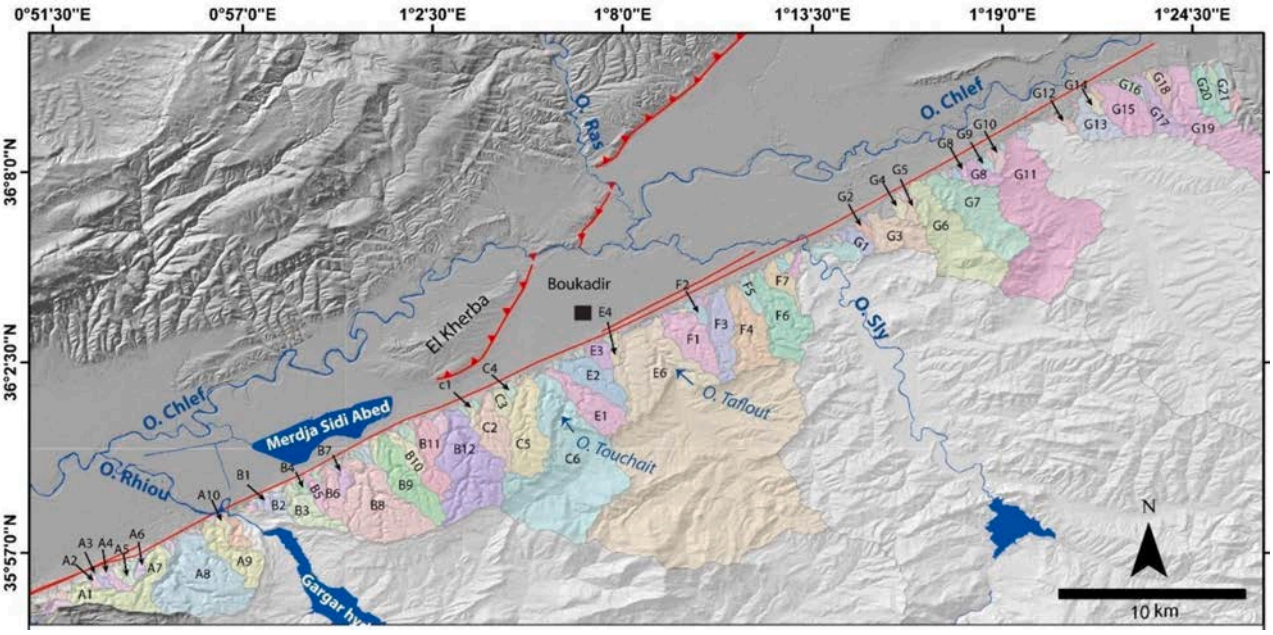

Fig. 4. Watersheds studied with hillshaded topography of TanDEM-X. The Relizane and Boukadir faults are represented.

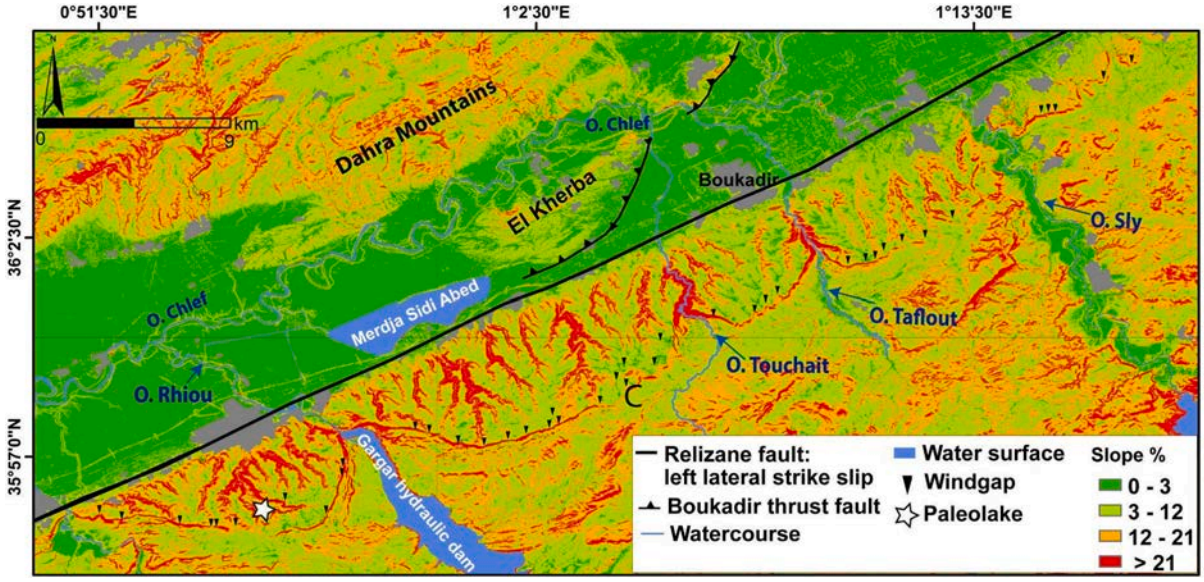

Fig. 5. Slopes map with the location of the main rivers, major faults of Boukadir and Relizane, and dry valleys extracted from the TanDEM-X digital elevation model. C represents the river capture.

formation of a valley results from concentrated water flow, which requires significant drained area upstream of the valley and slope gradient (Talling and Sowter, 1999), the presence of the wind gaps suggests a very different drainage organisation in the past. Only few south-flowing anaclinal (obsequent) rivers drain the platform, most of them initiate in the marly terrain close to the toe of the cuesta. The largest south-flowing river in the carbonates occurs on the edge of the B12 basin and results from a river capture by the Touchait watershed (C6 in Fig. 4).

Close to the cuesta, in the wind gaps and on the surrounding summits we can notice the presence of a reddish-brown soil that covered the calcrete (Fig. 9-left up). The soil is locally incised by gullies, allowing us to estimate that its thickness exceeds 3 m (length of the ravine escarpments in the soil >5 m on the Google Earth images; Fig. 9-right up). These gullies, that suddenly stop, have a similar orientation to the fracture network (SW-NE) mapped by Moulana et al. (2022). We interpret the abrupt stop of these incisions as water karstic losses (Fig. 9-right bottom).

The soil gradually disappears downstream and disappears in the valley bottoms a few hundred metres away from the cuesta, where incision increases and only the calcrete outcrops. Elsewhere on the platform reddish-brown clay material is only found in solution pipes (Moulana et al., 2022), that are centimetric to metric vertical dissolution conduits. We interpret this reddish-brown soil as evidence of a paleosoil that must have covered the entire platform. This paleosoil was later eroded and preserved only in solution pipes. At the outlets of the stream draining the platform we can notice that the valleys widen a little and are covered by a red soil.

C. Karstic features

The carbonate platform exhibits several marks of karstic processes, such as metric-sized shelter caves, present on practically every valley edge. They are arranged in staircase steps and attributed to river incision, some of them indicating paleo-river levels and others marking paleo-flow base levels of the endokarst (Moulana et al., 2022). In the latter case, they would correspond either to remnants of ancient caves brought to the surface by erosive surface processes or to perched and dried resurgences following the incision of river valleys, the lowering of the water table, and the uplift of the platform during the Plio-Quaternary induced by transpressive movement (Meghraoui, 1988).

The distribution of the shelter caves across the platform is heterogeneous. Along a given channel, the shelter caves are present only in the areas where the valleys are V-shaped without a thick alluvial cover, and mostly absent in upstream and downstream part of the drainage characterized by wider plate-shaped valleys (Fig. 9-left bottom) covered by soil (Fig. 9). Moreover, the caves density is different between the different drainage basins. In the central zone of the platform, where the relief is maximum, shelter cave levels are more numerous (Fig. 10), implying a greater development of endokarst. The shelter caves are an indicator of the incision, indeed their elevation above the active channel is maximal in the area where the incision shown by the slope map is high (Figs. 3 and 10). On the Fig. 10, the transition between the area of high incision and large endokarst and the ones with lower incision and karst development, is abrupt and located near the Touchait River, suggesting a fairly localized deformation process at the origin of these variations.

D. Drainage network confined to the platform

The Boukadir platform exhibits a well-developed drainage network composed of more than fifty rivers forming a dendritic, relatively straight and homogeneous network, except for the SE-NW oriented stream in watershed B12 (Fig. 4). The sinuosity map confirmed the homogeneity of the network with only local variation associated to the slope break that derives from the genesis of the platform (Fig. S1). Laterally, the basin shapes, spacing, and sizes are relatively similar, with drained areas ranging from 0.6 km^2 to 4.4 km^2 and a median value of 1.4 km^2. Only the main rivers of the region: Sly, Taflout, Touchait, and Rhiou have different geometries as they are not confined to the platform and also drain the Ouarsenis mountain. The incision of the platform along their courses is significant, reaching up to 150 m, resulting in a separation of the platform into distinct slabs, each having a different slope and relief as highlighted by the swath profiles. The Touchait River also shows a change in the width of its valley near the documented slope break (Fig. 7 & black dashed line in Fig. 14).

4.2. Morphometry

In this section, we examine in a more quantitative way the drainage network. For all the rivers that flow only on the platform, we extract different parameters such as the presence of knickpoints, concavity indices (θ) and slope steepness (k_{sn}), and values of (χ), to describe thor

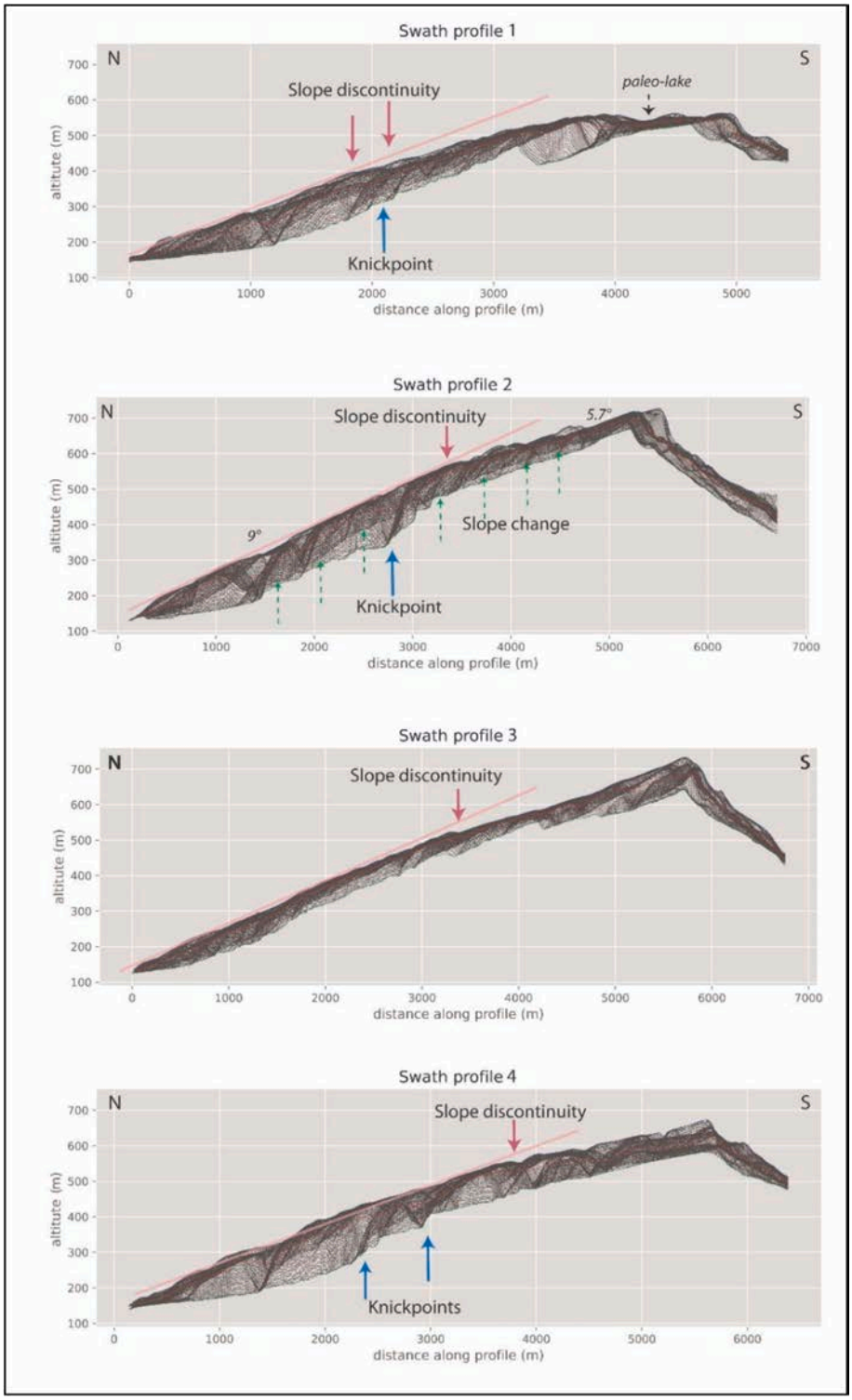

Fig. 6. Swath profiles located in Fig. 2-B, obtained from the Tandem-X DTM with sampling done every 14 m in a 1500 m large box. Slope discontinuities are indicated by a red arrow, knickpoint by blue arrows and bedding in swath profile 2 by green arrows. **Profiles 1 to 4**: Swaths obtained in the western and central zone. **Profiles 5 to 7**: Swaths obtained in the eastern zone.

equilibrium state. A river in equilibrium maintains a stable shape and gradient over time without significant incision or aggradation, and morphometric analysis seeks to pinpoint the origin of the observed disequilibrium. Although these morphometric analyses were carried out on all the watersheds, we will only present here the results of the most representative watersheds to avoid too much redundancy.

A. Longitudinal profiles and knickpoints

From the river profiles extracted in all of the watersheds, three main characteristic trends can be distinguished (Fig. 11). Firstly, the smallest watersheds located close to the foot of the platform present a concave-shaped distance-elevation profile, indicating that the streams in these

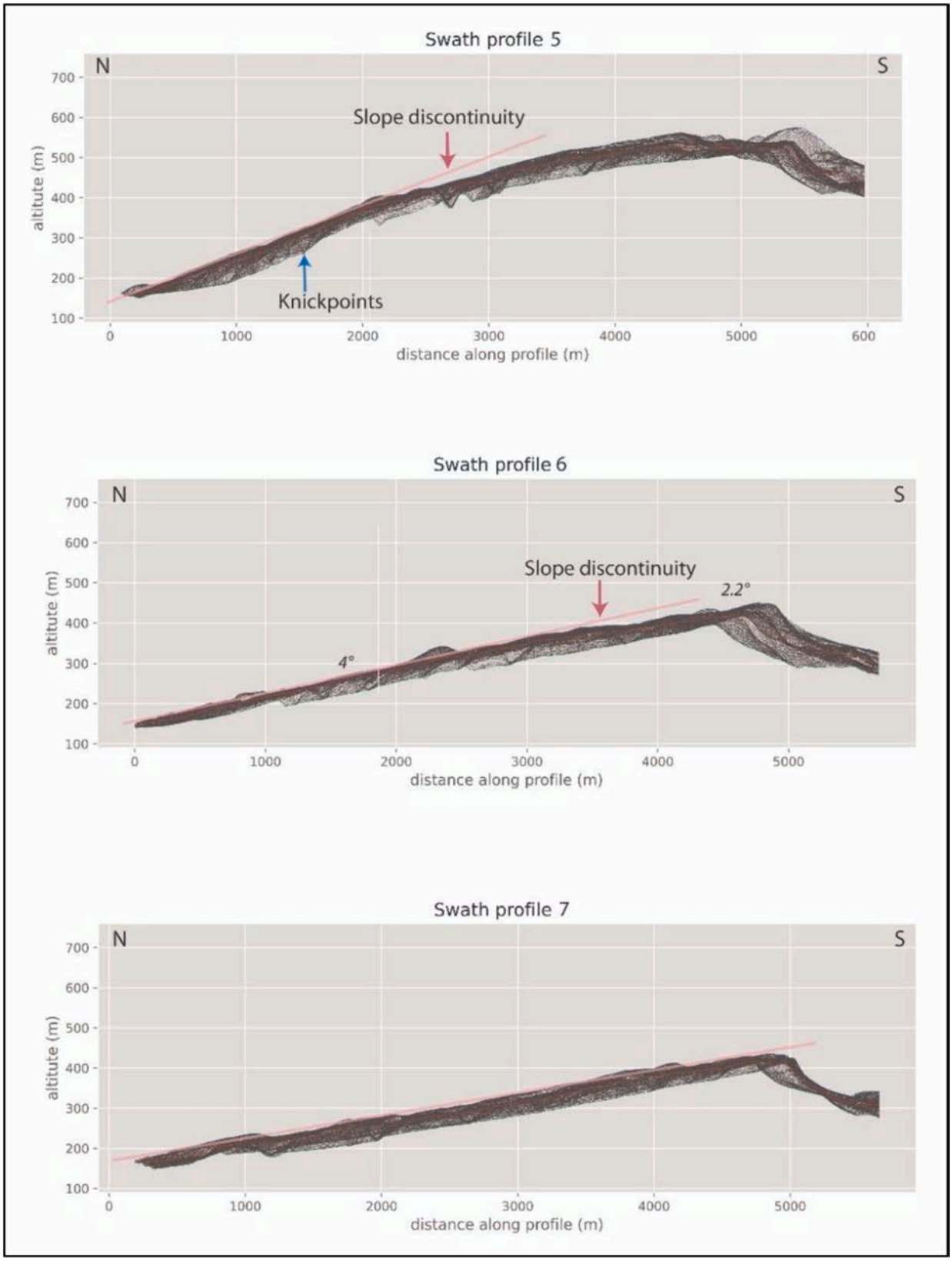

Fig. 6. (*continued*).

watersheds are in equilibrium (profiles of watersheds A10 and C1, Fig. 11). Secondly, the river profiles in the west exhibit characteristics that suggest they are not in equilibrium. The profiles are locally convex, and multiple knickpoints are distinguished by the TopoToolbox algorithm based on adjusting the concave upward profile with the actual stream. Finally, the river profiles in the east are the most difficult to interpret. No knickpoints are identified, but upstream convexities are still observed. These convexities are less pronounced than in the west,

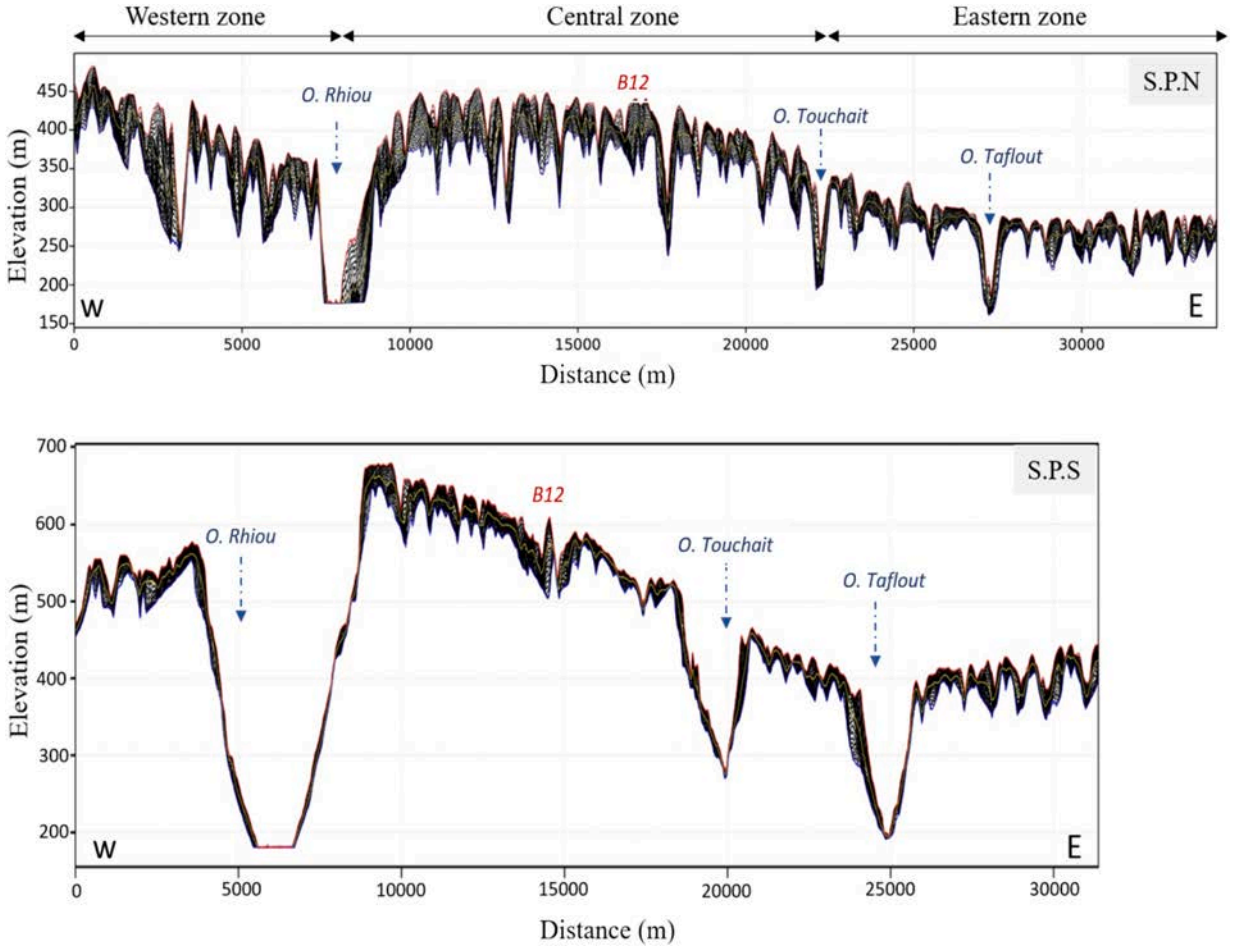

Fig. 7. East-West swath profiles located in Fig. 2-Up, carried out in the northern part of the carbonate platform (S.P.N) and at the back of the platform at the ridge level (S.P.S), obtained from the Tandem-X.

but they suggest that the rivers have not really reached equilibrium as well.

Fig. 12 shows a map of all identified knickpoints separated into two classes: those associated with a step >13 m (white), which is the threshold for which river profiles are best reproduced during automatic detection of knickpoints, and those associated with a step >45 m (pink), which correspond to major discontinuities. We can note the presence of numerous knickpoints in the central and western zones compared to the eastern zone (Fig. 12). Two categories of knickpoints can be distinguished in terms of location. The first category is knickpoints located at confluences that separate high-perched tributaries from a main stream. These hanging valleys are particularly visible adjacent to the main rivers such as the Taflout and Touchait Rivers crossing the platform and locally in the downstream part of watersheds for some tributaries. The second category of knickpoints is located directly on the main channels of watersheds confined to the platform. They are mainly located west of the Oued Touchait and are aligned sub-parallel to the Relizane fault.

B. χ-elevation profiles

On the platform we observe several kinds of χ-elevation profiles, the typical ones are shown on Fig. 13. The small catchments at the foot of the platform display straight profiles (catchments A10 and C1, Fig. 13), confirming that they are in equilibrium, while larger catchments have convex χ-elevation profiles, defining a knickzone with different characteristics depending on the drainage basin. Here, we define the knickzone as a portion of the river profile localized above a sudden slope increase in the χ elevation profiles and presenting locally high channel steepness (Beeson and McCoy, 2020). Upstream of the knickzone, there is a general flattening of the χ elevation curves which become subparallel. In the following we compare the χ-elevation profiles with the local morphology to explain the χ variations and the drainage evolution.

The two smaller watersheds in equilibrium, A10 and C1, have the same morphology that differs from the one of the larger watersheds. They have always been confined to the platform and are less incised than the adjacent truncated valleys. They exhibit a straight V-valley profile without significant aggradation and soil development but are associated with shelter caves.

The watersheds B8, and B12 in the central zone display the highest knickzones. The section downstream of the knickzone is a plate-shaped aggrading valley with a well-developed soil, while the knickzone corresponds to a meandering V-shaped valley with knickpoints, characteristic of a very strong incision. The upstream parts of these channels are plate-shaped valleys, filled by a thick soil similarly to the top of the platform. Further to the east just west of the Touchait River, the χ-elevation profile of catchment C5 has the same characteristics as catchments B8 and B12 but with a smaller knickzone. We can notice that two tributaries without wind gaps located in the downstream part of catchment C5 have straight profiles and V-shaped valleys, suggesting either that they have reached equilibrium such as A10 and C1 watersheds or that they have been recently captured by the catchment C5.

Between the Taflout and Touchait Rivers, the χ-elevation profiles of catchments E1 and E2 show a transition in profile geometry. The westernmost χ profile, E1 exhibits a well-defined knickzone and has a similar morphology as B12 but less pronounced. While the E2 χ-elevation profile is more linear and fan-shaped, its knickzone is less marked

suggesting that this catchment is closer to equilibrium. E2 catchment is less incised compared to E1 (Fig. 4) and misses the upstream area with plate-shaped valley implying that E2 has always been confined to the platform and thus does not have exactly the same history as E1.

East of the Taflout River, the χ-elevation profiles of the F4 and F7 watersheds are much closer to equilibrium. The collinearity between the tributaries and the mainstream observed in the F7 watershed confirms this near-state equilibrium (Perron and Royden, 2013). Again, the difference in χ-elevation profiles are coherent with the morphology, F7 which is closer to equilibrium was always confined to the platform, whereas F4 is a truncated watershed with wind gaps. Moreover, on the GE images we can observe that in F4 the valley morphology evolved along stream similarly as the drainages more to the west, with the succession of an aggrading plate-shaped valley, an incised V-shaped valleys about ~1.3 km south of the Chélif Basin and upstream close to the wind gaps a widening of the soil covered valley. This indicates an incipient knickzone, suggesting that the catchment is not at equilibrium yet.

The χ-elevation profile of catchment G3 does not evidence a knickzone but flattens upstream. G3 is less incised than the other catchments and is characterized by a plate-shaped valley with thick red soils all along the main stream and wind gaps on the drainage head. The remaining disequilibrium visible in the profile of this catchment might be due to this truncation.

Finally, at the eastern end of the platform, the catchments G17 and G19 experience a different tectonic context; they are located in the hanging wall of El Asnam thrust. Their χ-elevation profiles evidence the impact of this tectonic structure. G17, which is further from the thrust, has a profile that tends towards equilibrium, with locally a small convexity, while the G19 profile is more convex and out of equilibrium. In terms of morphology, these catchments display a sudden transition from a plate-shaped to a more V-shaped valley, which is much more marked for G19 than in G17. The main difference with the other catchments is that the valleys are still covered by a continuous soil cover.

C. K_{sn} map

The regional map of k_{sn} values in Fig. 14 also shows an east-west lateral variation with an abrupt change located in the central part of the platform at the level of the Touchait River. This corresponds to the transition zone previously identified in the χ elevation profiles (E1/E2 in Fig. 13) and the transition between the central and eastern zones identified in the morphology (Fig. 7). East of Touchait, the k_{sn} values are generally low (between 100 and 500 $m^{2\theta}$), and are higher west of Touchait (between 500 and 900 $m^{2\theta}$) coinciding with the higher relief (Figs. 7 and 14). Watersheds with low k_{sn} values are more stable than those with high k_{sn} values (Snyder et al., 2000). The k_{sn} results agree with the analysis of the out of equilibrium watersheds.

D. χ map

The analysis of the chi map in Fig. 15 allows us to understand the dynamics of the watershed divide migration (Willett et al., 2014). An equilibrium between two neighbouring watersheds is highlighted by homogenous χ values on either side of the watershed boundary (Winterberg and Willett, 2019). On the contrary, different χ values highlight unbalanced areas, the drainages with lower χ values correspond to regions where erosion is stronger than uplift, making them aggressors, and the drainages with higher χ values are considered as victims (Willett et al., 2014).

We focus essentially on the water divides at the cuesta location, to investigate the large-scale evolution of the platform. In the eastern part, where the platform has the lowest relief and slope, the drainage on the platform shows on average higher χ values than the one flowing south of the cuesta. This arrangement is consistent with the morphology in this zone, which suggests regressive erosion and migration of the watershed divide towards the north (Fig. 15-A1). On the contrary, in the west, where the slope is steeper the contrast of χ values shows higher values for the southern rivers compared to the ones on the platform, indicating a migration of the watershed divide towards the south, which is not realistic considering the presence of a very pronounced cuesta in this zone (Fig. 15-A2). This suggests that there is an external phenomenon in relation with tectonics that creates and maintains this imbalance.

In the western part we also observe the presence of southward anaclinal flows at the top of the platform and a capture of part of B12 basin by the Touchait watershed (Figs. 4 and 15). Those morphologies are consistent with the expected regressive erosion for a cuesta morphology but not with the direction of watershed evolution indicated by the chi map in the area (Fig. 15- A2). This contradiction suggests that the process at the origin of the disequilibrium of the drainage network in the western part of the platform is probably quite recent, that is why morphologies associated with the regressive erosion along the cuesta are still visible.

It should be noted that in the area of the capture, depending on the adjacent watershed considered, the direction of watershed divide migration varies (Fig. 15-A2), with migration towards the north for the basins to the east (C2, C5) and towards the south for the B12 basin to the west. This suggests that the imbalanced area is limited to the section of the platform between the Rhiou River and the river of watershed B12. Moreover, it suggests that the processes leading to this disequilibrium has a relatively localized origin as we do not have the same behaviour between two neighbouring watersheds.

5. Interpretation

5.1. Formation of the cuesta

The current morphology of the cuesta and the formation of dead valleys or wind gaps at the rear of the platform (Figs. 5, 8 and 9) is the result of two processes. The cuesta morphology derives from differential erosion. The marly terrains deposited from the Langhian to the Messinian, outcropping south of the cuesta, are less resistant and erode faster than harder more resistant carbonate terrains protected by a calcrete. Over time, the less resistant marls were eroded away, leaving the more resistant carbonate materials as elevated features in the landscape. This is a classic case of relief inversion that has also been observed in the sedimentary basins of Morocco, where the Pleistocene terraces covered with a thick calcrete and resting on marls are perched high in the landscape (Kaemmerer and Revel, 1991; Stokes et al., 2007; Rixhon et al., 2017). In case of relief inversion due to differential erodibility we expect the depth of the valley to correlate with the thickness of the erodible substrate, which is what we observe (Figs. 3 and 4).

Moreover, the cuesta elevation varies laterally, while the carbonates of the platform were deposited at similar water depths suggesting that the platform was probably deformed post-deposit with different amplitudes. The central zone between Rhiou and Touchait Rivers is the highest and thus the most deformed (Fig. 7), which is consistent with the significant change in incision (Fig. 4).

5.2. Deformation characteristics

The morphometric observations realised on the Boukadir platform help to characterize its deformation. The χ-elevation profiles suggest that the platform deformation corresponds to a variable tilt (Figs. 13 and S4). This interpretation is based on the numerical landscape evolution models of Beeson and McCoy (2020) that characterized the geomorphic signature of the transient fluvial response to tilting using 1-D river longitudinal profile evolution models. They demonstrate that tilting creates unique geomorphic signatures distinct from those induced by uniform uplift or catchment changes in relation with capture and headwater truncation. According to their model, the χ-elevation convex profiles that we observed on the Boukadir platform and the associated knickzone morphology can only be explained by a relatively strong

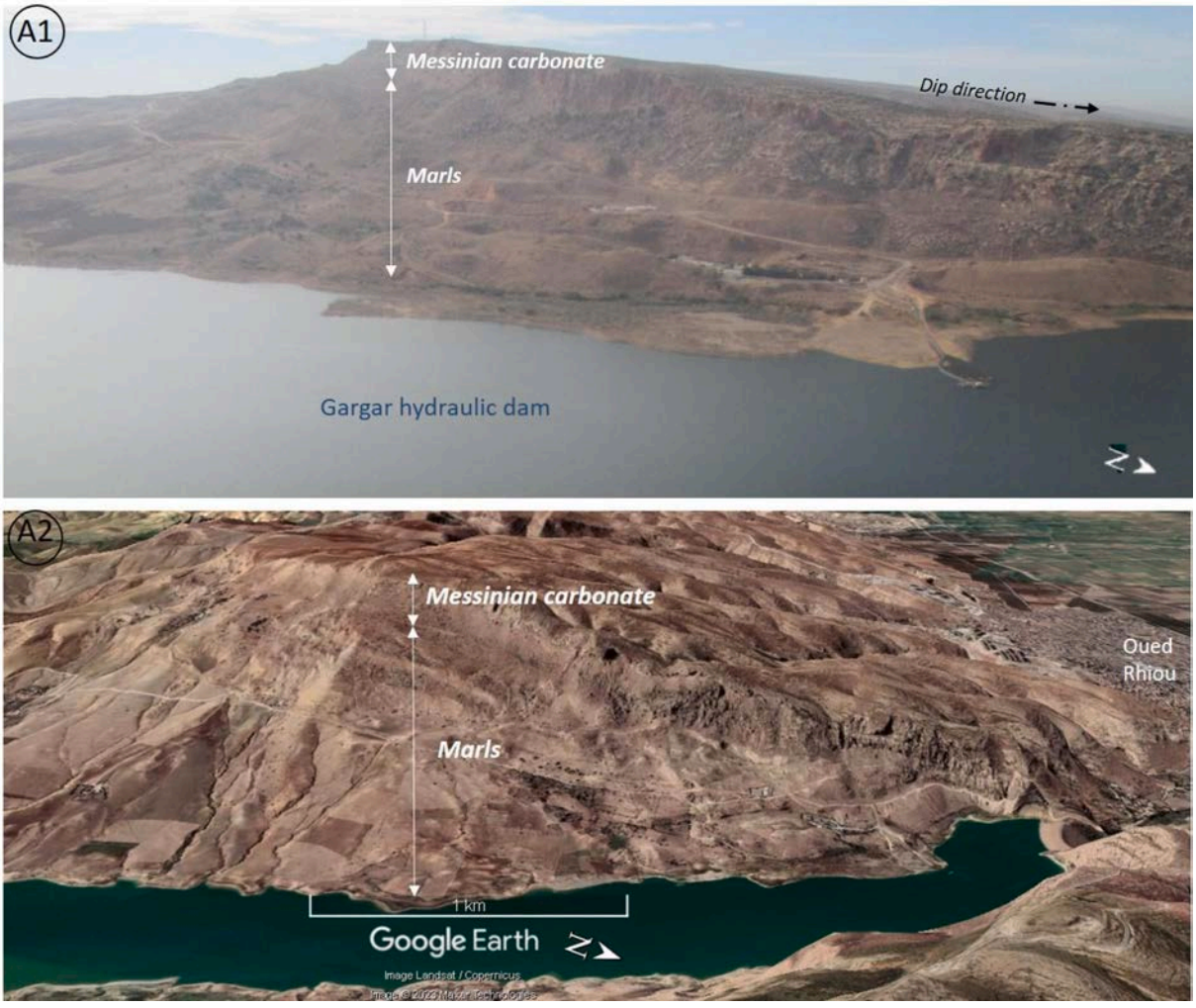

Fig. 8. A1. Field photograph and A2. Google Earth image showing the morphology of the cuesta and the carbonate platform to the west of Rhiou River.

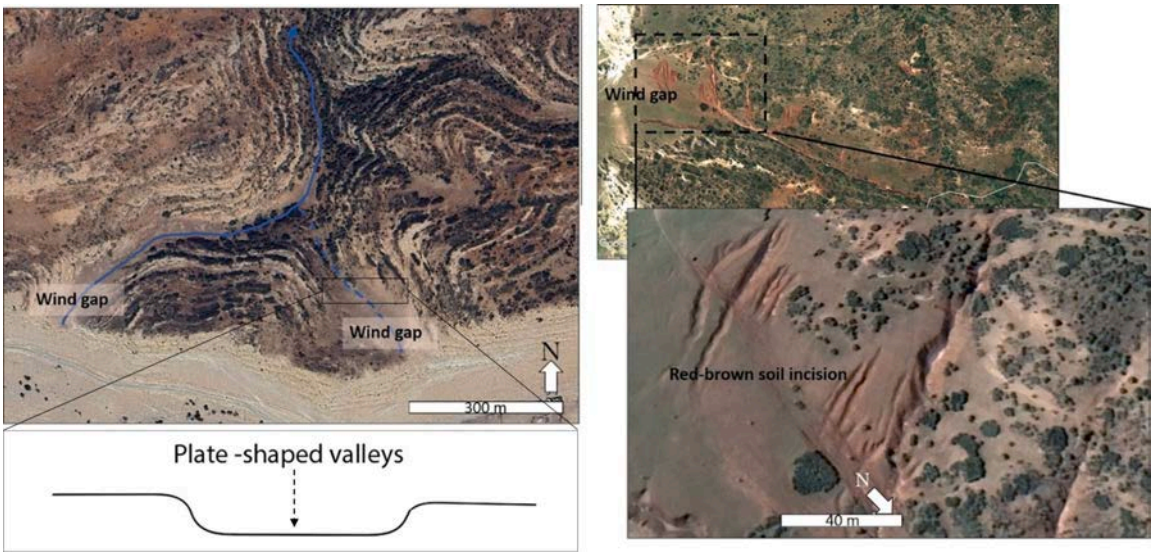

Fig. 9. Left up. Wind gaps mapped in the upstream part of the platform just north of the cuesta on Google Earth images. **Left bottom.** Plate-shaped valley representation. **Right up.** Preserved reddish-brown soil in the upstream part of the platform with local gullies. **Right bottom.** Zoom on the gullies, showing the thick reddish-brown soil and their sudden stop implying the occurrence of karstic losses.

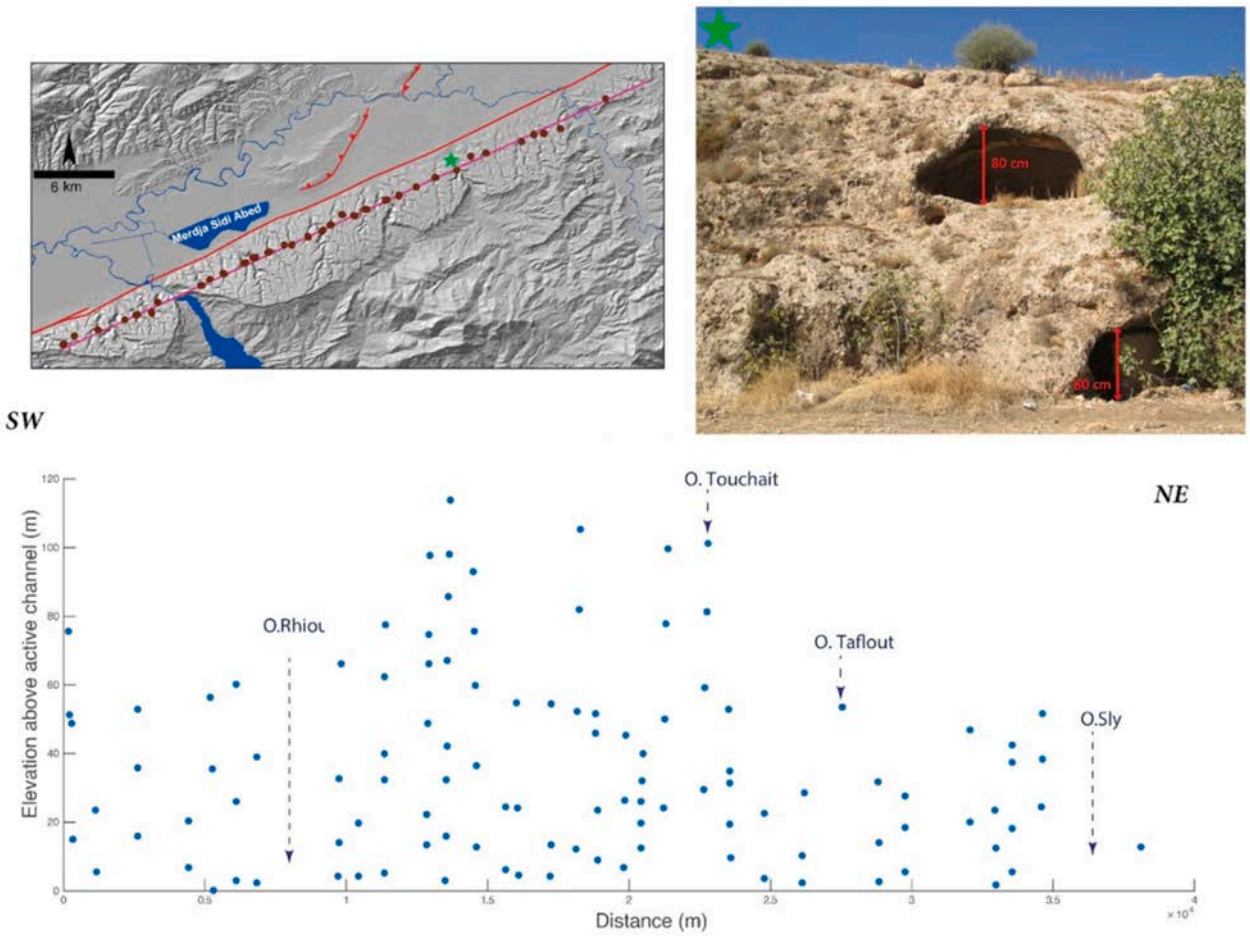

Fig. 10. Elevation difference between the shelter caves mapped using satellite imagery and the active channel at the same location as a function of their E-W location along a projection line in pink on the inset map. Top right: a field photograph of the shelter cave, about 80 cm high. The green star indicates the location of the photo.

tilting (Figs. 13 and S4). Such tilting also agrees with the other observed morphologic features such as the geometry, slope, and altitude variations. In general, the deformation seems higher in the central part of the platform, for example relief and incision that is higher in the central zone compared to the eastern zone (Fig. 5) and the knickzone height and amplitude are more pronounced in the central part of the platform, implying that this area has been more strongly deformed (Beeson and McCoy, 2020). Moreover, the fracture mapping on the platform by Moulana et al. (2022) evidenced the presence of fault offsets only in the central zone at the back of the platform associated with sediment accumulation in the hanging walls. Other morphometric variables are coherent with this interpretation, as the k_{sn} values that are proportional to uplift rates for homogeneous terrain lithology and can be used to determine tectonically induced perturbations (Kirby and Whipple, 2001; Mathew, 2016). Here, the k_{sn} map in Fig. 14 shows a sudden increase from east to west in the area around watershed B12, implying a higher uplift and tilt in the west. The χ map (Fig. 15) also indicates an imbalanced drainage network along the cuesta west of the Touchait River, with a migration of the divide in the opposite direction of regressive erosion, suggesting that the process that has deformed this part of the platform is still ongoing or at least recent. Thus, at least in the central part of the platform, these morphometric parameters point to a rapid deformation of the platform by tilting, probably during the Quaternary.

Finally, the geometry and drained areas of the investigated watersheds does surprisingly not seem affected by the gradient of deformation. Indeed, the density of drainage normally reflects the relative competition between fluvial (advective) and hillslope (diffusive) processes (Perron et al., 2008) and is a function of relief, precipitation, and erosion rates (Tucker and Bras, 1998). So, the drainage density generally changes markedly with the tilting of deformed surfaces, as evidenced in growing anticlines deforming the topographic surfaces (e.g. Talling and Sowter, 1999). This is not observed here, suggesting asynchrony of the two processes at work, namely drainage network incision and platform deformation. In this case, changes are observed at the scale of individual rivers rather than at the watershed scale. This is probably an indicator of weak deformation, because for a stronger deformation, even well-defined basins would be affected and have their limits changed. Another factor potentially preventing the modification of the catchment geometry is the fact that the lithological context had changed between the basin formation and the beginning of the tilting. Indeed, the valleys are inherited from the period before the cuesta formation, while the tilt is more recent and intervene after the formation of the calcrete at the top of the platform that is not easily erodible.

5.3. Knickzone and knickpoints

We observed that generally the knickpoints are collocated with the largest knickzones, suggesting a relation between these two features (Fig. 13). Indeed, the watersheds B8 and B12 have the highest knickzones (>200 m) and contain the most knickpoints, while east of Taflout River, where the convexities in the χ-elevation profiles are low, knickpoints are absent. Knickpoints are preferentially localized at the limits of the knickzones marked by the largest changes in elevation in χ-elevation profiles. In particular, the largest knickpoints (>45 m) occur only in the upper part of the knickzones where a large change in incision and valley morphology take place: from plate-shaped to V-shaped valleys.

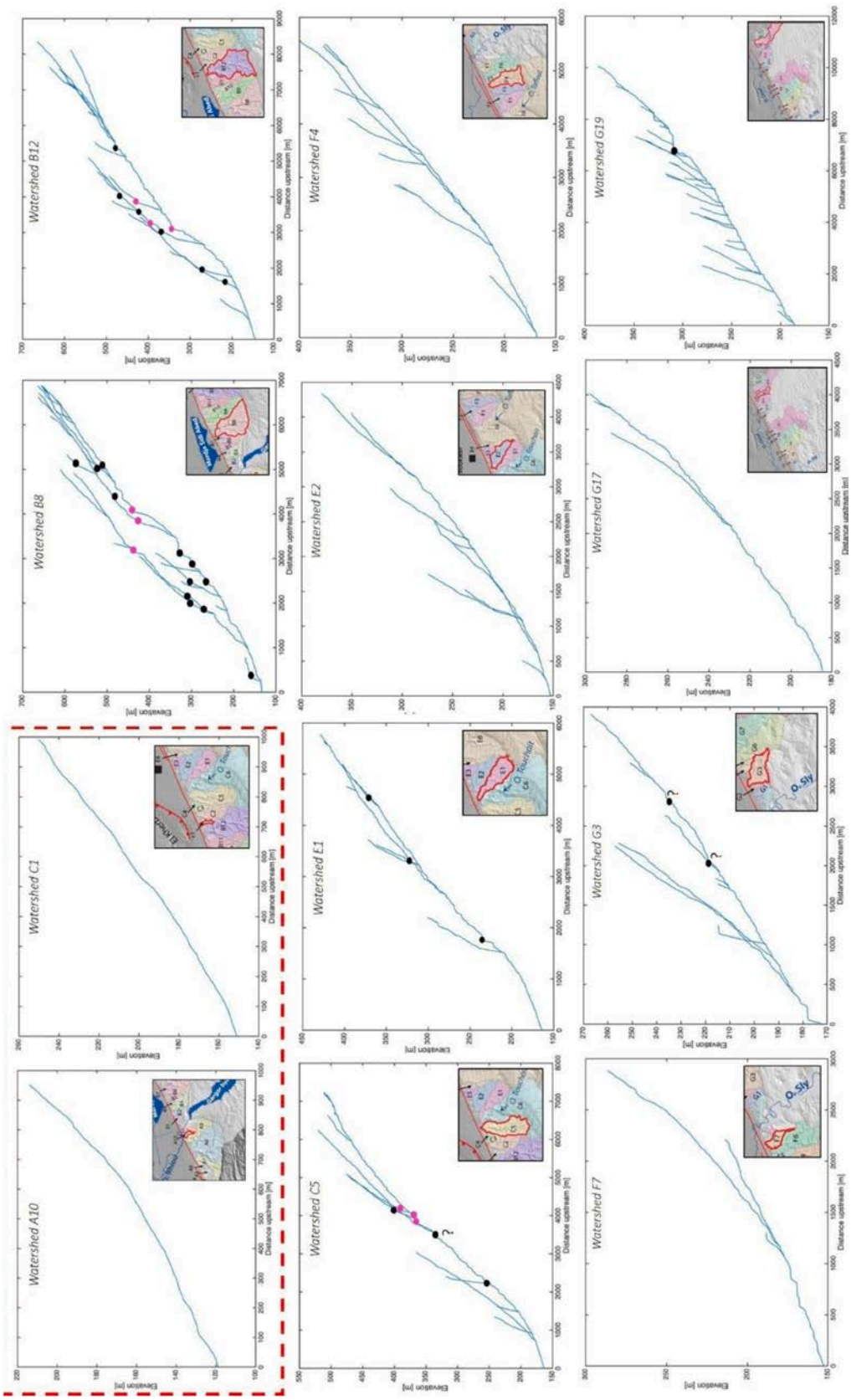

Fig. 11. Distance/Elevation profiles of some watersheds from west to east of the study area, with knickpoints (in black and pink dots) obtained independently using MATLAB's TopoToolboxs. The red dotted frame encompasses the two watersheds A10 and C1, which illustrate the state of equilibrium without knickpoints.

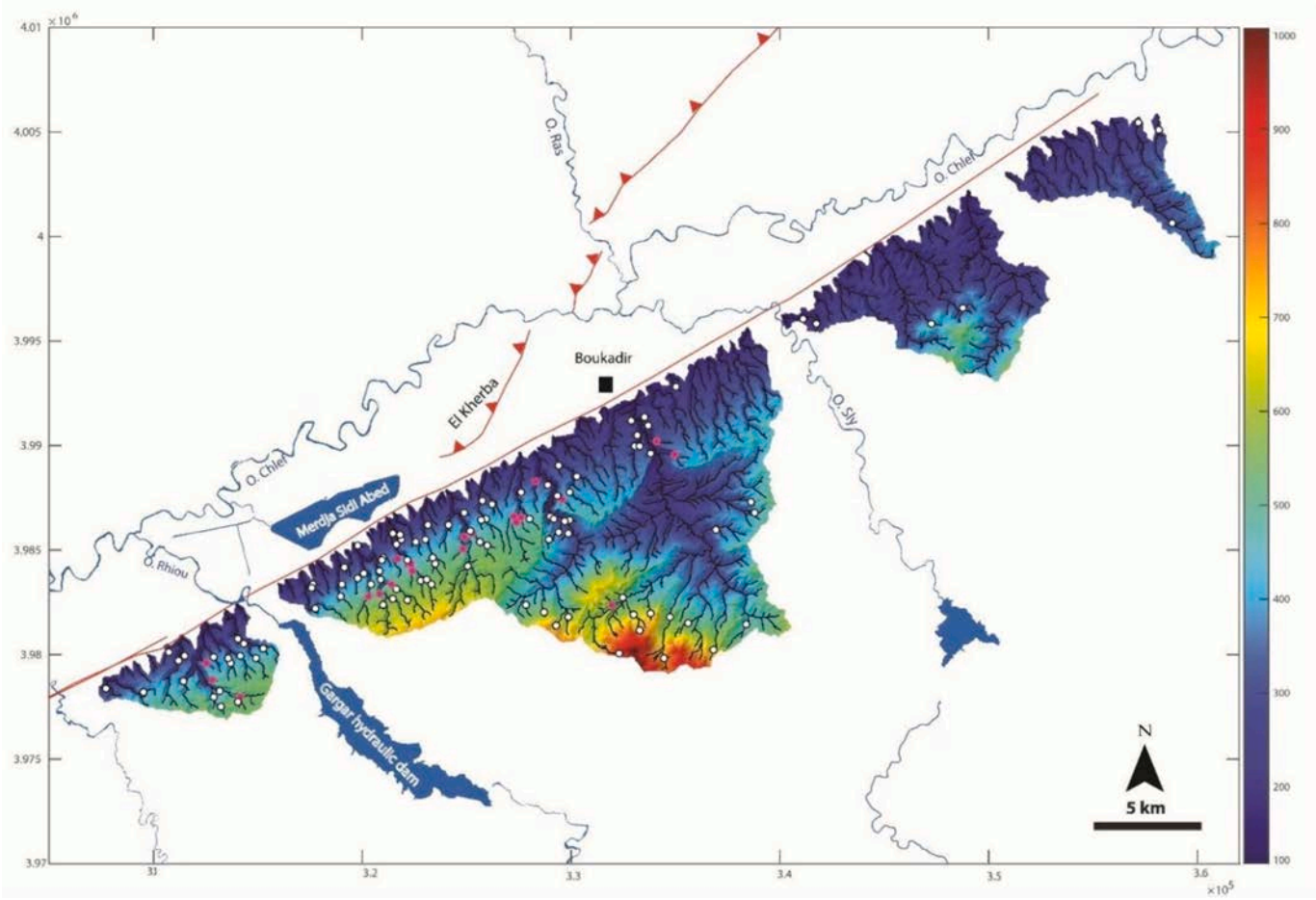

Fig. 12. Knickpoints map of the study area on the topographic background obtained using MATLAB's TopoToolbox. White dots represent knickpoint with steps >13 m. Pink dots represent knickpoint with steps >45 m.

The location of the small knickpoints at the confluence between the main rivers and their tributaries suggests that they are related to differential incision. Incision is a function of drainage area and bedload (Sklar and Dietrich, 2004). Thus, the small hanging valleys above the Taflout River can be related to the largest incision by this perennial river compared to its ephemeral tributaries. Moreover, there is a large variation in bedload between the two types of rivers because the Taflout River drains quartz-rich terrains south of the platform, whereas its hanging tributaries are restricted to the carbonate platform covered by a calcrete, whose erosion provides insignificant bedload. The differential erosion is probably also increased by the endokarstic drainage. Indeed, the mainstream corresponds to the local base level, when it lowers, the underground drainage developed which impacts the surface tributaries and delays their incision (Mather, 2000; Antón et al., 2012).

The other knickpoints may have a link with lithological differences. Indeed, the plate-shaped valley at the top of the platforms are composed of compact and homogeneous Lithothamnium carbonates, but near the top of the knickzones, at the knickpoint locations, we observe the appearance of a much more friable facies, the bioclastic facies (Fig. 16). When a more erodible bioclastic facies is exposed in the riverbeds, this leads to a knickpoint amplification. Moreover, the Google Earth images analysis also reveals that these knickpoints are associated with exsurgences and thus with the endokarst. The regressive erosion associated with the tilting has disrupted the functioning of the endokarst and underground flows, by exhuming part of the subsurface conduits (Fig. S5) and creating resurgences at the knickpoints location (Fig. 16). The mapping of shelter caves in a tributary of catchment 'B12' comprising two small knickpoints (~10 m) reveals that the resurgences strongly promote incision downstream of knickpoints (Fig. S2). Through this mechanism, a stronger geomorphological expression of these topographic steps can occur.

In conclusion, the knickzones, identified on the χ-elevation profiles of the Boukadir platform, are related to the tilting while the knickpoints are strongly linked to the surface regressive erosion and the endokarst. The latter are not related to a localized tectonic disturbance but rather to the change of incision gradient triggered by the tilting of the area. These karstic knickpoints are mostly related to lithological changes and resurgences due to erosion. They are not a priori prone to classical upstream migration. From that perspective, knickpoints in such karstic zones might not be representative of a tectonic uplift but rather of the erosive processes and the activity of the underground drainage system.

5.4. Origin of the tilting

We identify two possible origins regarding the tilt. First, it can be related to the differential compaction of the underlying marls. Indeed, marls can compact very strongly (Maillart and Beaudoin, 1989; Hunt and Fitchent, 1999), the degree of compaction depending on their thickness. In our case, the thickness of marls is highly variable. In the basin, drilling shows the presence of >1300 m of marls (Moulana et al., 2021) and we observed strong lateral variations of the marls thickness at the back of the carbonate platform (Fig. 2). To the southwest of the Rhiou River, the platform rests on <500 m of marls, which have been deposited on marine sandstone of the Oligocene (Figs. 2, 8). Eastward, the thickness of the marls decreases until it disappears east of the Sly River (Fig. 2). Based on the observation made by Tavani et al. (2018) in

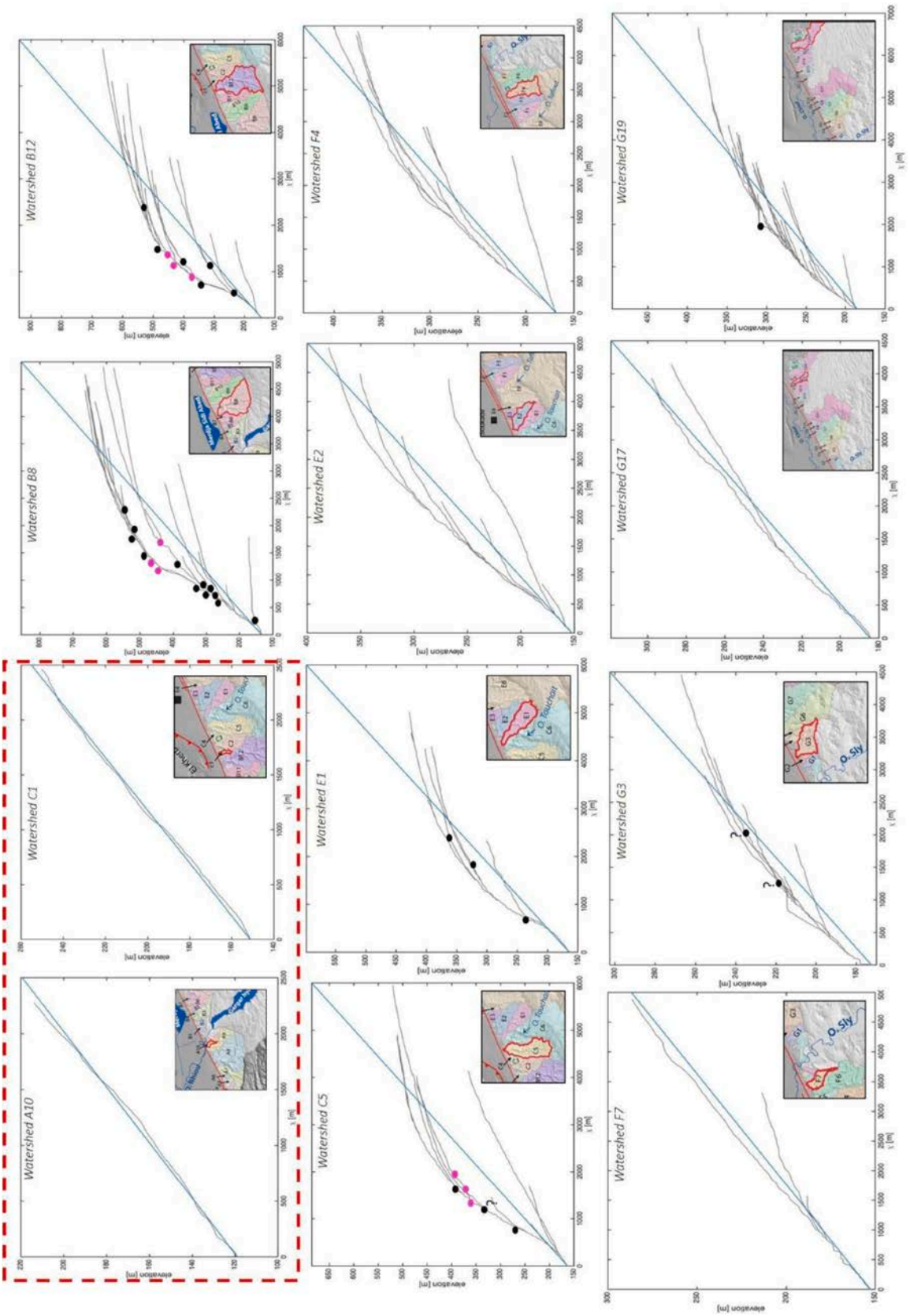

Fig. 13. χ/elevation profiles of some watersheds from west to east of the study area with black and pink dots indicating the knickpoints from Fig. 11 obtained independently using MATLAB's TopoToolbox. The red dashed frame encompasses the two watersheds "A10 and C1" that illustrate the equilibrium state.

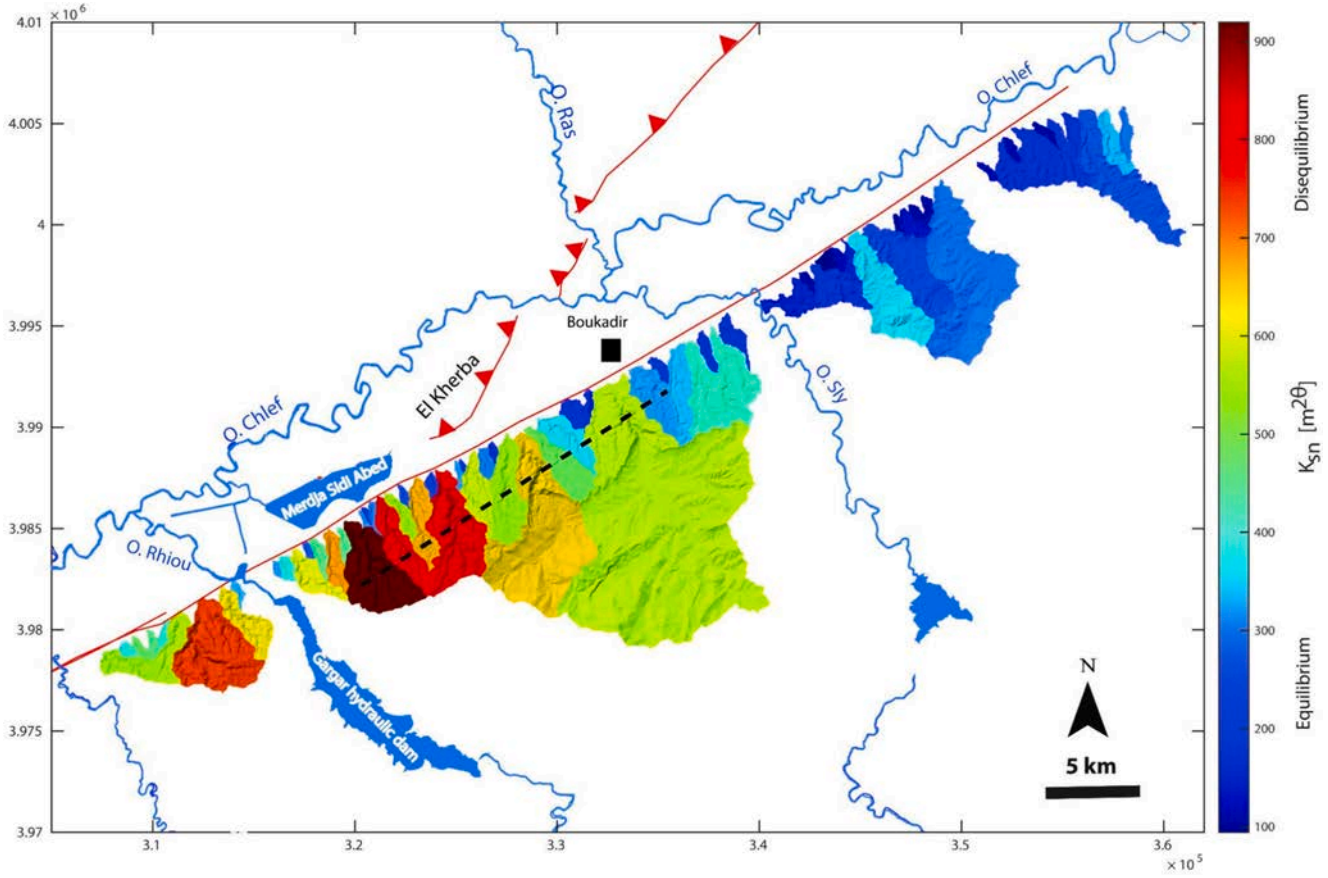

Fig. 14. K_{sn} map of the study area obtained using MATLAB's TopoToolbox. The redder the color, the more the watershed is in a state of disequilibrium, and the bluer the color, the more the watershed is in a state of equilibrium. The black dashed line represents the slope break.

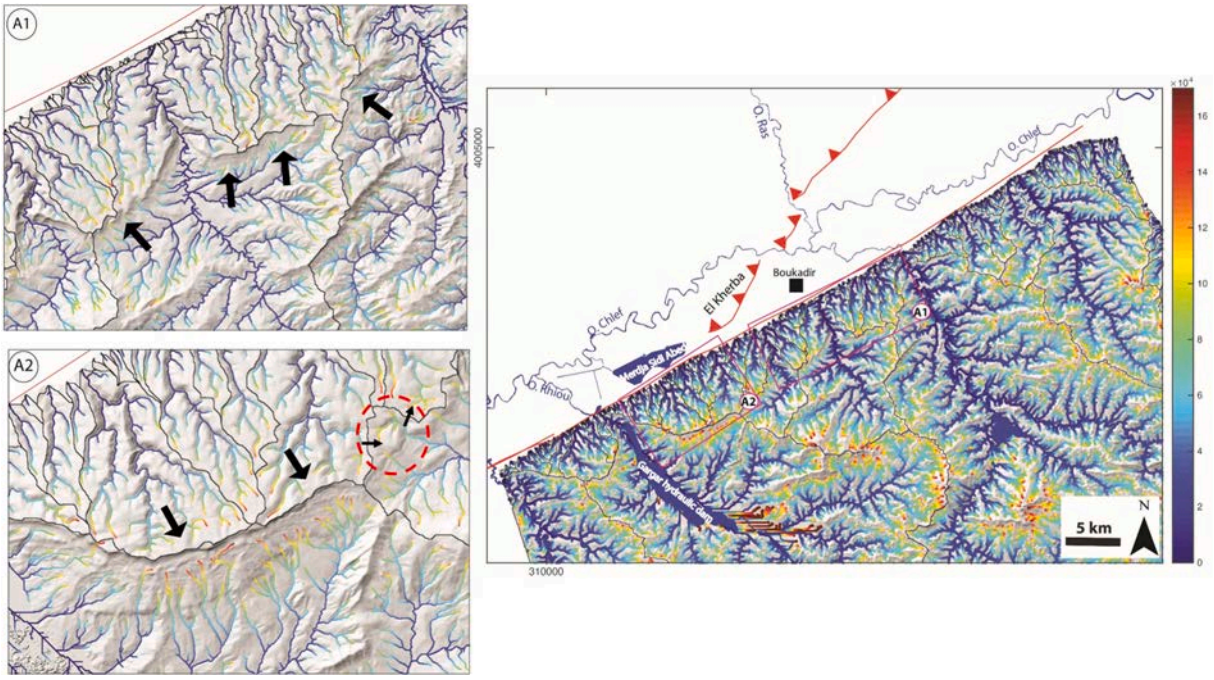

Fig. 15. χ map of the study area, the color code is based on the value of χ at each pixel point of the river. **A1.** Zoom on the eastern part of the χ map at Taflout River. Black arrows indicate the direction of water divide migration (S-N). **A2.** Zoom on the western part of the χ map at Touchait River. Black arrows indicate the direction of water divide migration (N-S). The red dashed circle indicates the main capture. The direction of water divide migration at this capture is indicated by black little arrows.

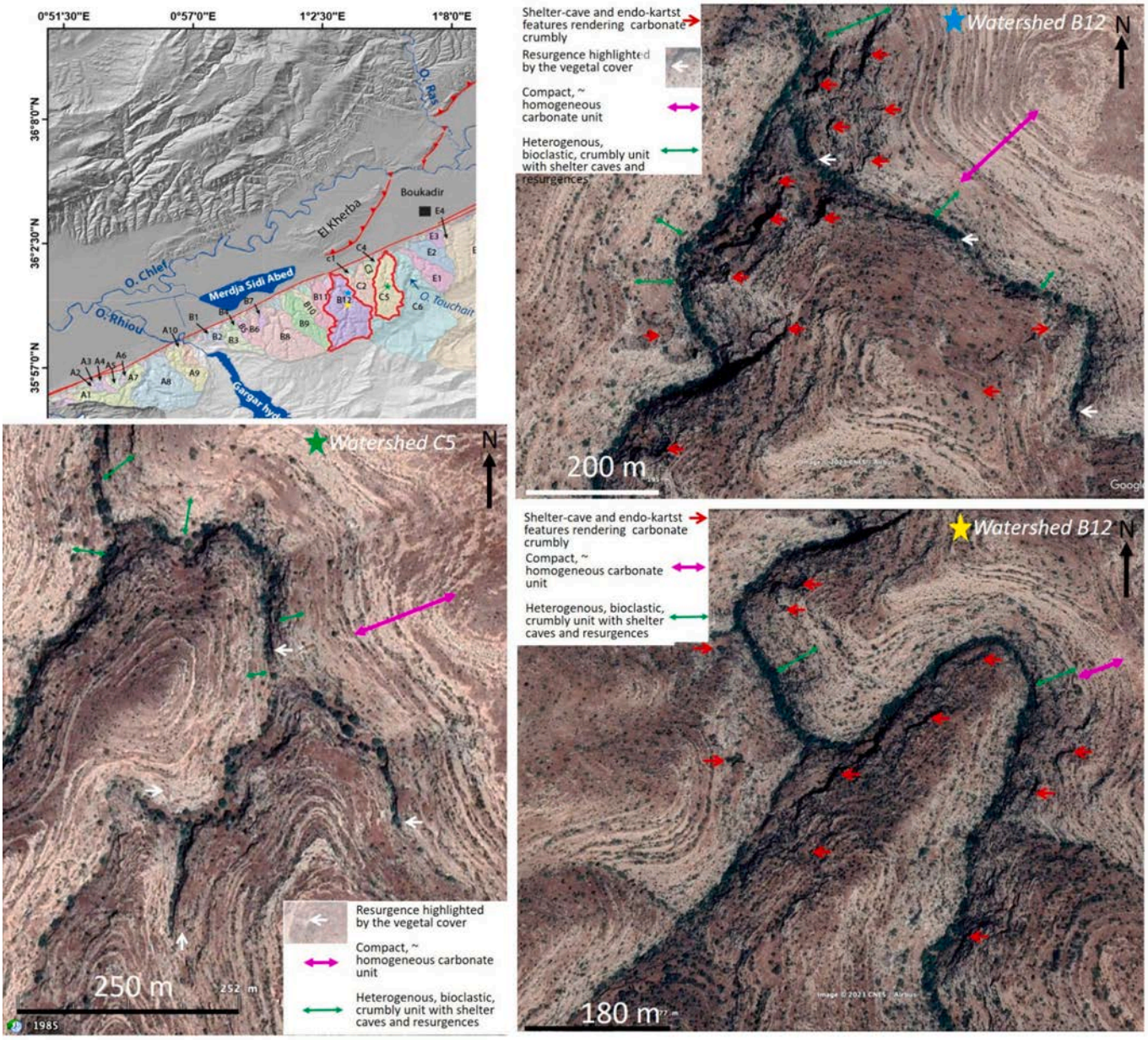

Fig. 16. Google Earth images in the knickzone areas showing the occurrence of resurgences (white arrows), shelter caves (red arrows) in the watersheds C5 and B12 (located in Fig. 12). The gray double-sided arrow represents the Lithothamnium carbonate unit, and the black double-sided arrow represents the bioclastic carbonate unit.

the Lurestan region in Iran, a thicker marl deposit in the basin would favour the tilting of the platform towards the basin. In the same way, the thickening of the sedimentary cover (carbonate at the platform and alluvium in the basin) from the cuesta to the Chélif basin might participate in the differential compaction. In addition, the Boukadir thrust and the associated anticline growth may have generated gravitational forces large enough to cause marl deformation or creep towards the south, facilitating the tilting of the platform. We conclude that the omnipresence of the tilting can be explained by the differential compaction of the marls, but the lack of knowledge about the precise 3D-geometry of marls does not allow us to model it.

The deformation field related to the compaction and deformation of the underlying marls is expected to evolve continuously along the platform. This is in contradiction with the morphological and morphometric observations indicating an abrupt spatial change in incision (Fig. 5) and deformation (k_{sn} map Fig. 14, and χ map Fig. 15) in the central region in line with the El Kherba anticline. We thus conclude that another process might intervene in the central region leading to a more intense deformation locally. It might be related to the diffuse propagation of the Boukadir thrust towards the southwest below the platform. To further test this hypothesis, we looked at the χ-elevation profile of the G19 drainage affected by the El Asnam reverse fault (Fig. 13). This profile shows a similar pattern as the ones located between the Rhiou and Touchait River, which confirms the hypothesis of a deformation related to the Boukadir reverse fault. We finally consider that tectonic deformation affecting the central region of the platform is subsequent to the initial thrust motion along the Boukadir Fault and therefore relatively recent.

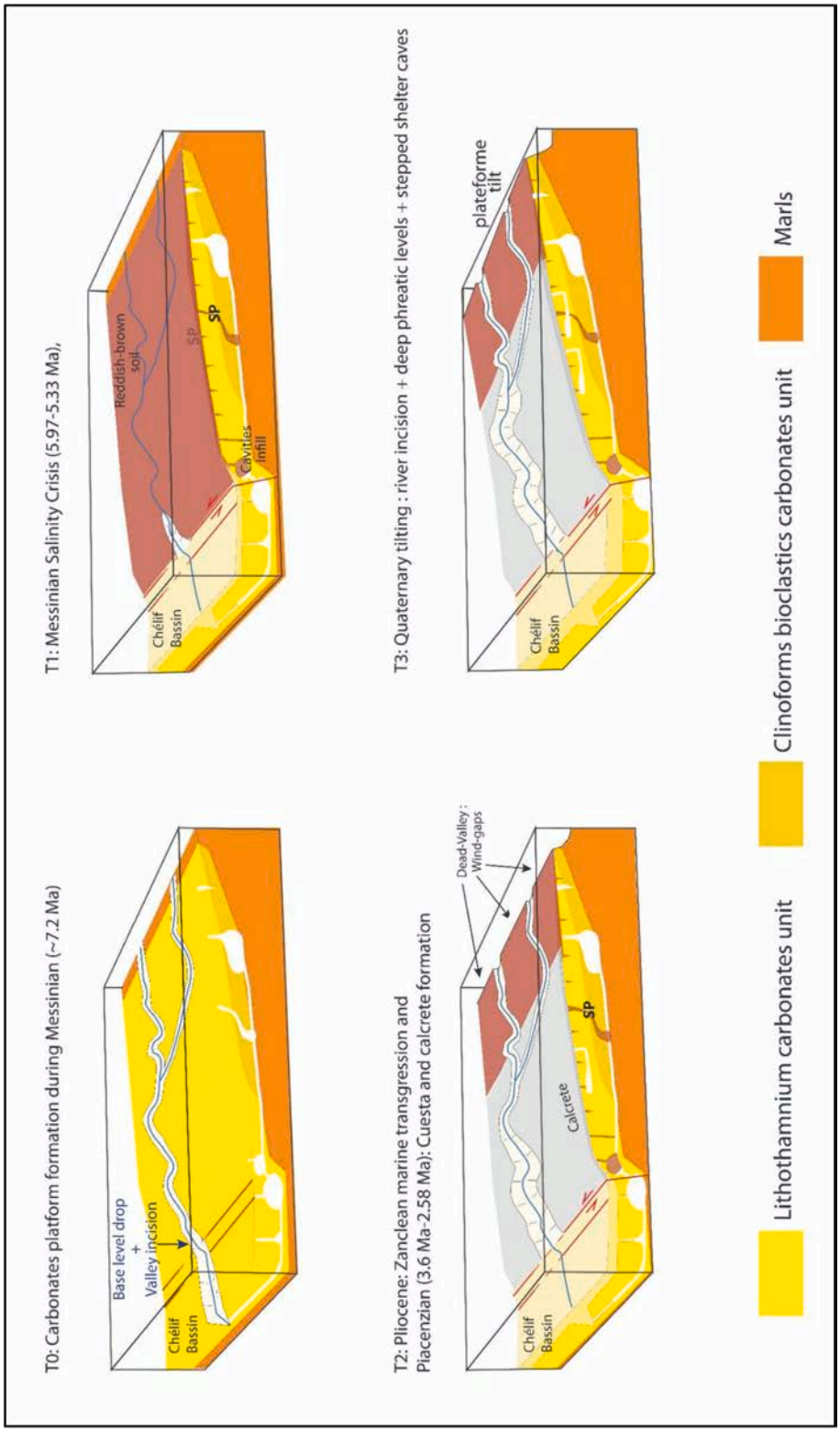

Fig. 17. Paleogeographic evolution of the Boukadir carbonate platform from Messinian in 1 to the Quaternary in 4.

6. Discussion

6.1. Evolution of the carbonate platform of Boukadir

All the analyses carried out allow us to present a paleogeographic reconstruction of the evolution of the Boukadir carbonate platform (Chélif Basin) since its formation (Fig. 17).

This carbonate platform began to form in the Messinian (~7.2 Ma) in the context of an inner ramp with a shallow high-energy marine environment and high sediment productivity. The platform was deposited on marly deposits that started to deform under the weight of the platform. A first bioclastic unit with clinoforms was deposited, followed by a second unit of Lithothamnium carbonates (Moulana et al., 2021). The deposit morphology is marked by a slight change in slope.

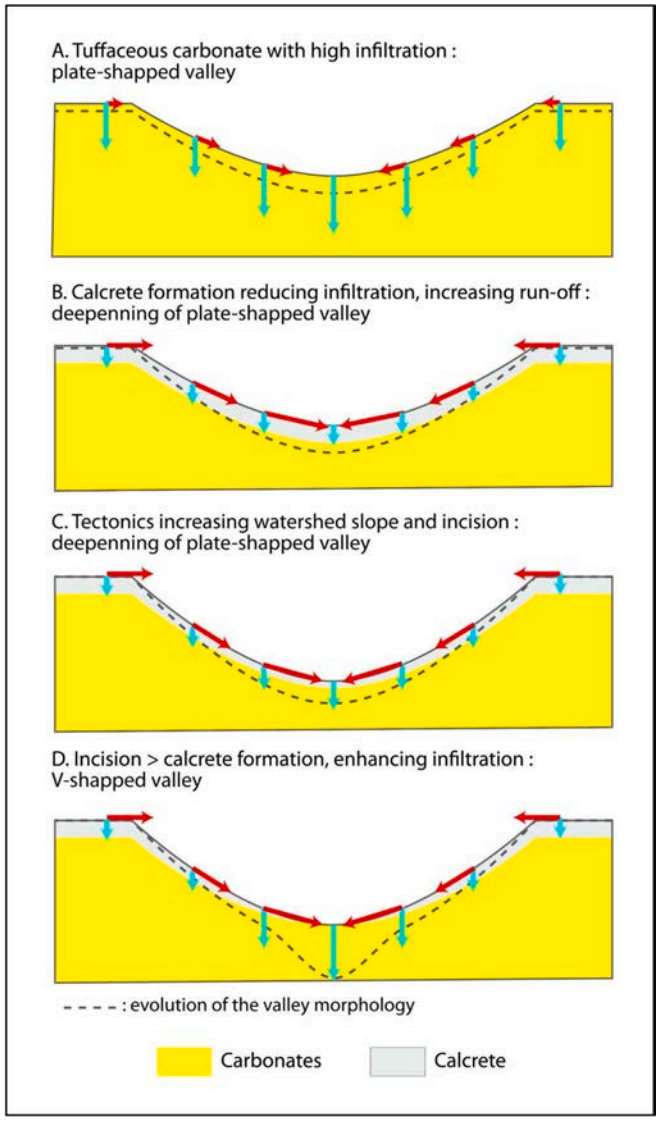

Fig. 18. Drainage evolution model in a porous carbonate terrain in a semi-arid environment.

During the Messinian Salinity Crisis (5.97–5.33 Ma), the lowering of the Mediterranean's base level (−1500 m) disconnected the marginal sea occupying the Chélif Basin from the Mediterranean. The base level of the Chélif Basin also dropped, and gypsum deposits typical from this period formed at the previously marly depocenter of the basin, located north of Boukadir (Roveri et al., 2014; Naimi et al., 2020; Moulana et al., 2021). The drop in base level has resulted in the emergence of the platform and the formation of a hydrographic network deeply incising the formerly marine terrains. At that time, there was a direct connection between the platform and the Ouarsenis relief southward, susceptible to generate a significant flow concentration to trigger an incision. The newly established river network includes the four main rivers that now traverse the area, as well as a NNW-oriented secondary cataclinal network, flowing from the southern Ouarsenis reliefs. This secondary drainage network flowed on the marine Eocene deposits of the relief and crossed the Langhian-Messinian marls and the Messinian carbonate platform and marls; the cuesta did not exist at that time. In the study area, the impact of this crisis is evidenced by the presence of paleo-canyons at the level of the four main rivers, revealed by drilling and geophysical prospecting-based sections (Moulana et al., 2022). The drop in base level also caused deep karstification, which later led to the collapse sinkhole of the RN4 between cities of Oued Sly and Boukadir.

After the Messinian Salinity Crisis, at the beginning of the Pliocene, the Zanclean marine transgression (Belhadji et al., 2008; Atif et al., 2008; Arab et al., 2015) led to the filling with marine or lacustrine clays, of the highly incised valleys in the carbonate piedmont (e.g., the paleo-Touchait and the paleo-Taflout) and deep cavities (Moulana et al., 2022). The reflooding of the Chélif Basin would have enhanced marine influence, including cooler and more moderate climates along its surrounding, and the expansion of vegetation cover. These more humid conditions are documented widely in the Maghreb region (Bédir et al., 1996; Mannaï-Tayech, 2006; Méon and Tayech, 1986; Tayech, 1984). During this period of biostasy, the reddish-brown soil developed on the whole carbonate platform. This soil is visible today mostly in the upper part of the platform (Fig. 9), in some valley bottoms and inside solution pipes (Moulana et al., 2022). The compressive tectonics related to the oblique convergence between Africa and Eurasia started to affect the studied region (i.e. Meghraoui et al., 1988; Rosenbaum et al., 2002). The Relizane fault, which structures the southern edge of the basin and determines the contact between the carbonate piedmont and the basin, was active during this period.

The next period is the Piacenzian (3.6 Ma–2.58 Ma) that is marked by an increase in seasonality and aridification. There was an expansion of grassland replacing some of the forested areas (Leroy and Dupont, 1994; deMenocal, 1995; Trauth et al., 2009; Novello et al., 2015). It was thus a period of rhexistasy, where the decrease in vegetation cover led to an increase of erosion. This period is also characterized by the occurrence of the Piacenzian Climatic Optimum (3.3–3 Ma) (Salzmann et al., 2011). In Algeria, the Piacenzian Climatic Optimum is marked by the development of a first thick layer of calcrete (Alonso-Zarza, 2003; Chellat et al., 2014, Fig. S3), dated at 3.2 Ma at the Oued Boucherit site (near city of Sétif) located ~375 km southeast of our site (Duval et al., 2021). The previously deposited reddish-brown soil covering the whole platform would have been eroded in its northern steeper part and is only preserved in flat places in some valley bottoms or in solution pipes (Moulana et al., 2022).

The calcrete favored differential erosion between the platform and the more marly terrain to the south, which led to the formation of the cuesta and, consequently, the appearance of the dead-end valleys perched at the top of the platform. The drainage pattern of pre-existing rivers was modified and led to the formation of south oriented anaclinal rivers (Lock et al., 2006; Burberry et al., 2007). Only the largest rivers: Rhiou, Touchait, Taflout and Sly, continue to flow through the platform, while the secondary network is cut off from its sources further south. Therefore, incision along streams having their headwater at the cuesta location decreases significantly. So, the difference in incision between the four main rivers and the secondary network becomes significant, which may explain the presence of hanging valleys. Finally, during this period, the NNE-SW compressive deformation intensified during this period and led to its progressive closure of the Chélif marine marginal Basin and its disconnection from the Mediterranean Sea at the end of the Pliocene. It is at this time that the Boukadir and the El Asnam thrust faults formed, while the lateral motion of the Relizane fault decreases (Meghraoui et al., 1986, 1996; Derder et al., 2011). The El Kherba anticline is also established in relation with the Boukadir thrust (Meghraoui et al., 1986).

During the Quaternary, continental sedimentation filled the Chélif Basin burying the Relizane Fault, the direction of compression changed from NNE-SSW to NNW-SSE (e.g. Meghraoui et al., 1986), and the rapid tilt of the platform started. This deformation is the source of the knickzones visible in the χ-elevation profiles and of the strong incision of the hydrographic network on the platform. The tilting induced river incision, leading to a deepening of the phreatic levels and creating stepped shelter caves (Moulana et al., 2022). This fluvial incision also disrupted the endokarst creating new phreatic levels. This tilt is more pronounced in the central zone this is due to a combination of factors, on one hand the differential compaction of the underlying marls, on the other hand the highest deformation aligned precisely with the

southwestern extension of the Boukadir thrust, suggesting an impact of the thrust in the platform deformation. This high deformation centred between the Rhiou and Taflout Rivers is thus interpreted to result from the diffuse propagation of the Boukadir thrust under the platform.

6.2. Drainage evolution model in a porous carbonate terrain: tectonics versus climatic impact

Our study evidenced that the evolution of the drainage network in a porous environment in the Maghreb area is profoundly influenced by two key factors: climatic conditions and tectonic forces. They interact to shape valley morphology and hydrological dynamics, creating a complex and constantly evolving landscape. We propose the following schematic evolution model of a carbonate platform in the Maghreb region (Fig. 18).

First, in a carbonate porous environment, water infiltration is diffuse, while run-off remains relatively low. This influences the valley morphology, giving them a wide plate-shape. The infiltration is enhanced when a soil develops, because it provides additional CO2, and increases the carbonate dissolution. In the Maghreb area, soil does not develop only in situ through the process of residual dissolution, there also are significant external soil inputs of aeolian loess (Yaalon and Ganor, 1973; Yaalon, 1987; Jahn et al., 1991; Bronger and Bruhn-Lobin, 1997; Muhs et al., 2010). Therefore, soils are thicker than expected given the semi-arid climate of this region, and the resulting carbonate dissolution is larger.

Second, during the Plio-Quaternary, strong climate changes have modified the state of the earth's surface (Fujioka et al., 2005). In the Maghreb region, this climatic period was typically characterized by an increased aridification and a pronounced seasonality. The associated weathering gave rise to a gradual transformation of the porous medium into a layer of indurated carbonate known as calcrete (Goudie, 1983; Esteban and Klappa, 1983; Wright and Tucker, 1991). This induration changed the ratio of infiltration versus runoff, which have favored the deepening of the pre-existing drainage network during the pluvial period of the Quaternary. The increase of runoff also led to a concentration of the surface water in the bottom of the valleys which strengthened locally the dissolution, and thus localized the erosion in valley bottoms. Moreover, in a second time the increased runoff and water concentration also changed the ratio of in situ soil formation by weathering versus soil erosion, with the erosion prevailing in the valley's bottoms. All these processes led to a deepening of the previously wide plate-shaped valleys.

Third, the tectonics acts as an amplifier of runoff and incision (Lague et al., 2003). When the tectonic activity is intense, the rate of incision exceeds that of calcrete formation, bringing the porous carbonates at the surface in the valley bottom. Even if this porous terrain locally greatly favors infiltration, its strong erodibility coupled with a still significant runoff triggers a high incision, which gives rise to V-shaped valleys. Moreover, the resulting erosion also brought the endokarst to the surface creating resurgences in the incised valleys (Harmand et al., 2017; Hercman et al., 2023). The resurgences reinforce the water discharge downstream and thus the incision, inducing morphological changes from plate-shaped to V-shaped valleys. For a limited tectonics the rate of calcrete formation stays high enough to limit the incision, thus the plate-shaped morphology persists.

The catchment size can also intervene in modeling the valley morphology when calcrete is covering it. In small watersheds, runoff stays too limited to affect the calcrete, resulting in less pronounced incision, contrary to the large watersheds, where the incision is pronounced. So small tributaries can be hanging above larger ones and knickpoints formed.

The proposed evolutionary model applies only to semi-arid climatic conditions. It is important to note, however, that porous carbonate formations found in higher latitude regions, such as the chalk of France, the UK and Belgium, exhibit distinct evolutionary patterns due to their significantly different climatic contexts, influenced by factors such as higher precipitation rates, vegetation cover and varying degrees of weathering and erosion as well as different impact of quaternary glacial-interglacial cycles (Rodet et al., 2006; Nehme et al., 2020; Farrant et al., 2023).

7. Conclusion

To better characterize the evolution of drainage networks in porous carbonate terrain, we study the Boukadir carbonate massif and its karstification in an active tectonic context. Using longitudinal river profiles analysis and more regional morphometric parameters, in combination with morphological analyses, we evidence a variable tilt of the platform as well as out-of-equilibrium drainage systems characterized by knickpoints and convexities. We interpret them in relation with present-day tectonic deformation processes, associated with differential compaction and karstic/weathering processes. We propose the following landscape evolution model: after the platform formation during the early Messinian, a deep karstification occurred, linked to the drastic variation of the base level associated with the Messinian salinity crisis (Moulana et al., 2022). At that time, the surface drainage network was established as well as the deep underground cavity network. Subsequently, platform evolution was mainly controlled by climatic and tectonic variations. The oblique convergence between Africa and Eurasia triggered a transpressive deformation. After a period of biostasy with soil development and river aggradation, the Pliocene climatic optimum leads to the beginning of calcrete development on the platform. This induces differential erosion between the platform and the surrounding areas, which leads to the formation of a cuesta and the disconnection of the platform drainage network from its initial sources, except for the four main rivers that remain cross-cutting. During the Quaternary, the deformation changed. The platform was deformed by tilting, as highlighted by the χ-elevation profiles of rivers. Morphological and morphometric analyses show lateral variations in this deformation, which is much more pronounced to the west than to the east. This variable tilt, affecting the whole southern border of the Chélif Basin, is probably partly due to differential compaction of the marls underlying the platform that changes laterally with the marls thickness variation. Nevertheless, the abrupt change in watersheds equilibrium aligned with the Boukadir Thrust suggests a diffuse propagation of the Boukadir thrust under the platform. Finally, we propose a more general model of drainage evolution as a function of climate and tectonics. Under semi-arid climatic conditions such as those of the Maghreb regions, the transition from a porous terrain to an indurated carbonate (calcrete) terrain has profound implications on drainage evolution, modifying infiltration, runoff and valley morphology. Tectonic activity acts as an amplifier of runoff and incision, leading to the transition from plate-shaped to V-shaped valleys. In addition, the size of the catchment plays a key role in the degree of incision, with smaller catchments experiencing less pronounced changes. These dynamic interactions between geology, climate and tectonics contribute to the complexity and constant evolution of the region landscape.

CRediT authorship contribution statement

Meriem L. Moulana: Writing – original draft, Methodology, Investigation, Formal analysis. **Marthe Lefevre:** Writing – original draft, Methodology, Investigation, Formal analysis. **Aurélia Hubert-Ferrari:** Writing – original draft, Supervision, Investigation.

Declaration of competing interest

The authors declare that they have no known competing financial interests or personal relationships that could have appeared to influence the work reported in this paper.

Data availability

Data will be made available on request.

Acknowledgments

The authors sincerely thank Mr. Camille EK for his invaluable assistance with the proofreading, corrections, and interpretation of the photos of the El Retaimia cave. Our sincere thanks go out to Ms. Sarah Robinet for her initial contribution to the TanDEM-X analysis and the morphometric analyses that were carried out. We express our gratitude to M. Meghraoui, D. Delvaux de Fenffe, and F. Boulvain for their fruitful discussions and feedback. Additionally, we acknowledge the constructive input of the GEOMORPHOLOGY editor, Martin Stokes, even though our paper was not accepted. This feedback has significantly contributed to the improvement of our paper, leading to a better presentation of our results and the development of the presented model in Section 6.2.

Appendix A. Supplementary data

Supplementary data to this article can be found online at https://doi.org/10.1016/j.geomorph.2024.109347.

References

Alonso-Zarza, A.M., 2003. Palaeoenvironmental significance of palustrine carbonates and calcretes in the geological record. Earth Sci. Rev. 60 (3–4), 261–298. https://doi.org/10.1016/S0012-8252(02)00106-X.

Anthony, D., Granger, D., 2007. An empirical stream power formulation for knickpoint retreat in Appalachian Plateau fluviokarst. J. Hydrol. 343, 117–126. https://doi.org/10.1016/j.jhydrol.2007.06.013.

Antón, L., Rodés, A., De Vicente, G., Pallàs, R., Garcia-Castellanos, D., Stuart, F.M., Bourlès, D., 2012. Quantification of fluvial incision in the Duero Basin (NW Iberia) from longitudinal profile analysis and terrestrial cosmogenic nuclide concentrations. Geomorphology 165, 50–61. https://doi.org/10.1016/j.geomorph.2011.12.036.

Arab, M., Bracene, R., Roure, F., Zazoun, R.S., Mahdjoub, Y., Badji, R., 2015. Source rocks and related petroleum systems of the Chelif Basin (western Tellian domain, north Algeria). Mar. Pet. Geol. 64, 363–385. https://doi.org/10.1016/j.marpetgeo.2015.03.017.

Atif, K.F.T., Bessedik, M., Belkebir, L., Mansour, B., Saint Martin, J.P., 2008. Le passage Mio-Pliocène dans le bassin du Bas Chélif (Algérie). Biostratigraphie et paléoenvironnements. Geodiversitas 30 (1), 97–116.

Azañón, J.M., Galve, J.P., Pérez-Peña, J.V., Giaconia, F., Carvajal, R., Booth-Rea, G., Jabaloy, A., Vázquez, M., Roldán, F.J., 2015. Relief and drainage evolution during the exhumation of the Sierra Nevada (SE Spain): is denudation keeping pace with uplift? Tectonophysics 663, 19–32. https://doi.org/10.1016/j.tecto.2015.06.015.

Ballesteros, D., Farrant, A., Sahy, D., Genuite, K., Bejarano, I., Nehme, C., 2023. Going with the flow: sedimentary processes along karst conduits within Chalk aquifers, northern France. Sediment. Geol. 452, 106422.

Bédir, M., Tlig, S., Bobier, C., Aissaoui, N., 1996. Sequence stratigraphy, basin dynamics, and petroleum geology of the Miocene from eastern Tunisia. AAPG Bull. 80 (1), 63–80. https://doi.org/10.1306/64ED8746-1724-11D7-8645000102C1865D.

Beeson, H.W., McCoy, S.W., 2020. Geomorphic signatures of the transient fluvial response to tilting. Earth Surf. Dyn. 8 (1), 123–159. https://doi.org/10.5194/esurf-8-123-2020.

Belhadji, A., Belkebir, L., Saint Martin, J.P., Mansour, B., Bessedik, M., Conesa, G., 2008. Apports des foraminifères planctoniques à la biostratigraphie du Miocène supérieur et du Pliocène de Djebel Diss (bassin du Chélif, Algérie). Geodiversitas 30 (1), 79–96.

Belkebir, L., Bessedik, M., Ameur-Chehbeur, A., Anglada, R., 1996. Le Miocène des bassins nord-occidentaux d'Algérie: biostratigraphie et eustatisme. In: Bulletin des Centres de recherches exploration-production Elf-Aquitaine. Mémoire, 16, pp. 553–561.

Bense, V.F., Gleeson, T., Loveless, S.E., Bour, O., Scibek, J., 2013. Fault zone hydrogeology. Earth Sci. Rev. 127, 171–192. https://doi.org/10.1016/j.earscirev.2013.09.008.

Bettahar, N., 2012. Effect of the Climate and Soil Characteristics on the Nitrogen Balance in the North of Algeria. In: Horticulture. IntechOpen.

Brives, A., Ferrand, M., 1912. Carte géologique de l'Algérie 1:50,000: 105. Alger : Service géologique de l'Algérie.

Bronger, A., Bruhn-Lobin, N., 1997. Paleopedology of Terrae rossae—Rodoxeralfs from quaternary calcarenites in NW Morocco. Catena 28 (3-4), 279–295. https://doi.org/10.1016/S0341-8162(96)00043-4.

Burbank, D.W., Anderson, R.S., 2001. Tectonic Geomorphology: A Frontier in Earth Science. Blackwell Science, Malden, Mass.. https://doi.org/10.2113/gseegeosci.19.2.198

Burberry, C.M., Cosgrove, J.W., Liu, J.G., 2007. Stream network characteristics used to infer the distribution of fold types in the Zagros Simply Folded Belt, Iran. J. Maps 3 (sup1), 32–45. https://doi.org/10.1080/jom.2007.9711027.

BURGEAP, 2004. Prospection géophysique à travers la région : HAMADNA - BOUKADIR. Wilaya de Relizane. Rapport définitif. Agence National Ressources Hydrauliques (ANRH), 57 pp.

Burns, S.J., Fleitmann, D., Matter, A., Neff, U., Mangini, A., 2001. Speleothem evidence from Oman for continental pluvial events during interglacial periods. Geology 29 (7), 623–626. https://doi.org/10.1130/0091-7613(2001)029<0623:sefofc>2.0.co;2.

Chellat, S., Djerrab, A., Bourefis, A., 2014. Les grés Mio-Pliocene de la région de Guerrara: analyse sedimontologique séquentielle et paléo-environnementale. Bull. Serv. Géol. Natl 25 (2), 1–21.

Crosby, B.T., Whipple, K.X., 2006. Knickpoint initiation and distribution within fluvial networks: 236 waterfalls in the Waipaoa River, North Island, New Zealand. Geomorphology 82 (1–2), 16–38. https://doi.org/10.1016/j.geomorph.2005.08.023.

D'Agostino, N., Jackson, J.A., Dramis, F., Funiciello, R., 2001. Interactions between mantle upwelling, drainage evolution and active normal faulting: an example from the central Apennines (Italy). Geophys. J. Int. 147 (2), 475–497. https://doi.org/10.1046/j.1365-246X.2001.00539.x.

deMenocal, P.B., 1995. Plio-pleistocene African climate. Science 270 (5233), 53–59. https://doi.org/10.1126/science.270.5233.53.

Derder, M.E.M., Henry, B., Amenna, M., Bayou, B., Maouche, S., Besse, J., Abtout, A., Boukerbout, H., Bessedik, M., Bourouis, S., Ayache, M., 2011. Tectonic evolution of the active "Chelif" basin (Northern Algeria) from paleomagnetic and magnetic fabric investigations. In: New Frontiers in Tectonic Research at the Midst of Plate Convergence Intech Publisher Book, 978-953-307-594-5, 2011. Intech Publisher, pp. 3–26.

Dewey, J.W., 1991. The 1954 and 1980 Algerian earthquakes: implications for the characteristic-displacement model of fault behavior. Bull. Seismol. Soc. Am. 81 (2), 446–467.

Dewey, J.F., Helman, M.L., Knott, S.D., Turco, E., Hutton, D.H.W., 1989. Kinematics of the western Mediterranean. Geol. Soc. Lond., Spec. Publ. 45 (1), 265–283. https://doi.org/10.1144/GSL.SP.1989.045.01.15.

Duval, M., Sahnouni, M., Parés, J.M., van Der Made, J., Abdessadok, S., Harichane, Z., Chelli Cheheb, R., Boulaghraif, K., Pérez-González, A., 2021. The Plio-Pleistocene sequence of Oued Boucherit (Algeria): a unique chronologically-constrained archaeological and palaeontological record in North Africa. Quat. Sci. Rev. 271, 107116 https://doi.org/10.1016/j.quascirev.2021.107116.

Ek, C., Mathieu, L., Lacroix, D., 1981. Croûtes et encroûtements calcaires en climat méditerranéen. L'exemple du bled Ouljamane (Maroc oriental). Actes du Colloque de l'Association des Géographes français : Formations carbonatées externes, tufs et travertins. Association française de Karstologie, mémoire n° 3, pp. 61–72.

Esteban, M., Klappa, C.F., 1983. Subaerial exposure environments. In: Shole, P.A., Bebout, D.G., Moore, C.H. (Eds.), Carbonate Depositional Environments, American Association of Petroleum Geologists. Memoir, 33, pp. 1–54.

Farrant, A.R., Maurice, L., Ballesteros, D., Nehme, C., 2023. The genesis and evolution of karstic conduit systems in the Chalk. Geol. Soc. Lond., Spec. Publ. 517 (1), SP517-2020 https://doi.org/10.1144/SP517-2020-126.

Flint, J.J., 1974. Stream gradient as a function of order, magnitude, and discharge. Water Resour. Res. 10 (5), 969–973. https://doi.org/10.1029/WR010i005p00969.

Fujioka, T., Chappell, J., Honda, M., Yatsevich, I., Fifield, L.K., Fabel, D., 2005. Global cooling initiated stony deserts in central Australia 2–4 Ma, dated by cosmogenic 21Ne-10Be. Geology 33, 993–996. https://doi.org/10.1130/G21746.1.

Gaillard, T., Hoyez, B., Hauchard, E., 2023. **Contribution of stratigraphy to groundwater motion understanding in chalk: examples of karstogenic horizons of the Pointe de Caux, France**. Geol. Soc. London, Spec. Publ. 517 (1), SP517–2020. https://doi.org/10.1144/SP517-2020-157.

Gaillard, T., Lasseur, É., Saïga, J., Dewez, T., Sizun, J.P., Collin, P.Y., 2018. Sédimentologie et pétrophysique de la craie–Impact sur les écoulements actuels dans la Pointe de Caux (France). Géologues 199, 25–28.

Gallen, S.F., Wegmann, K.W., Bohnenstiehl, D.R., 2013. Miocene rejuvenation of topographic relief in the southern Appalachians. GSA Today 23 (2), 4–10.

Goudie, A.S., 1983. Calcrete. In: Goudie, A.S., Pye, K. (Eds.), Chemical Sediments and Geomorphology. Academic Press, London, pp. 93–131.

Grohmann, C.H., 2005. Trend-surface analysis of morphometric parameters: a case study in southeastern Brazil. Comput. Geosci. 31 (8), 1007–1014. https://doi.org/10.1016/j.cageo.2005.02.011.

Hack, J., 1957. Studies of longitudinal stream profiles in Virginia and Maryland. USGS Prof. Pap. 249, 97.

Harkins, N., Kirby, E., Heimsath, A., Robinson, R., Reiser, U., 2007. Transient fluvial incision in the headwaters of the Yellow River, northeastern Tibet, China. J. Geophys. Res. Earth Surf. 112 (F3) https://doi.org/10.1029/2006JF000570.

Harmand, D., Adamson, K., Rixhon, G., Jaillet, S., Losson, B., Devos, A., Hez, G., Calvet, M., Audra, P., 2017. Relationships between fluvial evolution and karstification related to climatic, tectonic and eustatic forcing in temperate regions. Quat. Sci. Rev. 166, 38–56. https://doi.org/10.1016/j.quascirev.2017.02.016.

Hercman, H., Gąsiorowski, M., Szczygieł, J., Bella, P., Gradziński, M., Błaszczyk, M., Matoušková, S., Pruner, P., Bosák, P., 2023. Delayed valley incision due to karst capture (Demänová Cave System, Western Carpathians, Slovakia). Geomorphology 437, 108809. https://doi.org/10.1016/j.geomorph.2023.108809.

Hoffmann, D.L., Rogerson, M., Spötl, C., Luetscher, M., Vance, D., Osborne, A.H., Fello, N.M., Moseley, G.E., 2016. Timing and causes of North African wet phases during the last glacial period and implications for modern human migration. Sci. Rep. 6 (1), 36367 https://doi.org/10.1038/srep36367.

Horta, J.D.O., 1980. Calcrete, gypcrete and soil classification in Algeria. Eng. Geol. 15 (1–2), 15–52. https://doi.org/10.1016/0013-7952(80)90028-9.

Howard, A.D., Kerby, G., 1983. Channel changes in badlands. Geol. Soc. Am. Bull. 94 (6), 739–752. https://doi.org/10.1130/0016-7606(1983)94<739:CCIB>2.0.CO;2.
Hunt, D., Fitchent, W.M., 1999. Compaction and the dynamics of carbonate-plateform development: insights from the Permian Delaware and Midlands basins, Southeaust New Mexico and West Texas, U.S.A. In: Advances in Carbonate Sequence Stratigraphy: Application to Reservoir, Outcrops and Models. SEPM Special Publication n°63, pp. 75–106.
Jahn, R., Zarei, M., Stahr, K., 1991. Genetic implications of quartz in "Terra Rossa"-soils in Portugal. In: Proceedings of 7th Euroclay Conference, Dresden, pp. 541–546.
Kaemmerer, M., Revel, J.C., 1991. Calcium carbonate accumulation in deep strata and calcrete in Quaternary alluvial formations of Morocco. Geoderma 48 (1–2), 43–57. https://doi.org/10.1016/0016-7061(91)90005-E.
Karnik, V., 1969. Seismicity of the European Area, 1. D. Reidel, Dordrecht, Holland. (364 pp.).
Kirby, E., Whipple, K., 2001. Quantifying differential rock-uplift rates via stream profile analysis. Geology 29 (5), 415–418. https://doi.org/10.1130/0091-7613(2001)029<0415:QDRURV>2.0.CO;2.
Kirby, E., Whipple, K.X., 2012. Expression of active tectonics in erosional landscapes. J. Struct. Geol. 44, 54–75. https://doi.org/10.1016/j.jsg.2012.07.009.
Kirby, E., Whipple, K.X., Tang, W., Chen, Z., 2003. Distribution of active rock uplift along the eastern margin of the Tibetan Plateau: inferences from bedrock channel longitudinal profiles. J. Geophys. Res. Solid Earth 108 (B4). https://doi.org/10.1029/2001JB000861.
Krijgsman, W., Capella, W., Simon, D., Hilgen, F.J., Kouwenhoven, T.J., Meijer, P.T., Sierro, F.J., Tulbure, M.A., van den Berg, B.C.J., van der Schee, M., Flecker, R., 2018. The Gibraltar corridor: watergate of the Messinian salinity crisis. Mar. Geol. 403, 238–246. https://doi.org/10.1016/j.margeo.2018.06.008.
Lague, D., 2014. The stream power river incision model: evidence, theory and beyond. Earth Surf. Process. Landf. 39 (1), 38–61. https://doi.org/10.1002/esp.3462.
Lague, D., Crave, A., Davy, P., 2003. Laboratory experiments simulating the geomorphic response to tectonic uplift. J. Geophys. Res.: Solid Earth 108 (B1). https://doi.org/10.1029/2002JB001785. ETG-3.
Leroy, S., Dupont, L., 1994. Development of vegetation and continental aridity in northwestern Africa during the Late Pliocene: the pollen record of ODP Site 658. Palaeogeogr. Palaeoclimatol. Palaeoecol. 109 (2-4), 295–316. https://doi.org/10.1016/0031-0182(94)90181-3.
Lock, J., Kelsey, H., Furlong, K., Woolace, A., 2006. Late Neogene and Quaternary landscape evolution of the northern California Coast Ranges: evidence for Mendocino triple junction tectonics. Geol. Soc. Am. Bull. 118 (9-10), 1232–1246. https://doi.org/10.1130/B25885.1.
Maillart, J., Beaudoin, B., 1989. Compaction différentielle ou fracturation tectonique ? Faille et compaction. - 2ème Congrès Français de Sédimentologie, Paris, pp. 187–188.
Mannaï-Tayech, B., 2006. Les séries silicoclastiques miocènes du Nord-Est au Sud-Ouest de la Tunisie: une mise au point. Geobios 39 (1), 71–84. https://doi.org/10.1016/j.geobios.2004.08.003.
Mather, A.E., 2000. Adjustment of a drainage network to capture induced base-level change: an example from the Sorbas Basin, SE Spain. Geomorphology 34 (3–4), 271–289. https://doi.org/10.1016/S0169-555X(00)00013-1.
Mathew, M.J., 2016. Analyse morphotectonique et géomorphologique de la bordure nord de Bornéo (Malaisie). Doctoral dissertation. Université de Bretagne Sud.
Mathieu, L., Lacroix, D., Ek, C., Rassel, A., 1983. Sols et croûtes calcaires dans la Basse Moulouya intérieure (Maroc oriental). In: Recherches géographiques à Strasbourg, 22-23, pp. 97–109.
Mazzoli, S., Helman, M., 1994. Neogene Patterns of Relative Plate Motion for Africa-Europe: Some Implications for Recent Central Mediterranean Tectonics. In: Active Continental Margins—Present and Past. Springer, Berlin, Heidelberg, pp. 464–468. https://doi.org/10.1007/978-3-662-38521-0_19.
Meghraoui, M., 1982. Etude néotectonique de la région nord-est d'El Asnam: Relation avec le séisme du 10 Octobre 1980. PhD. Paris VII University, Paris, France (in French).
Meghraoui, M., 1988. Géologie des zones sismiques du Nord de l'Algérie. Paléosismologie, Tectonique active et synthèse sismotectonique. Thèse de Doctorat d'Etat. Université de Paris-Sud, centre d'Orsay, France, 356 pp.
Meghraoui, M., Cisternas, A., Philip, H., 1986. Seismotectonics of the lower Cheliff basin: structural background of the El Asnam (Algeria) earthquake. Tectonics 5 (6), 809–836. https://doi.org/10.1029/TC005i006p00809.
Meghraoui, M., Philip, H., Albarede, F., Cisternas, A., 1988. Trench investigations through the trace of the 1980 El Asnam thrust fault: evidence for paleoseismicity. Bull. Seismol. Soc. Am. 78 (2), 979–999. https://doi.org/10.1785/BSSA0780020979.
Meghraoui, M., Morel, J.L., Andrieux, J., Dahmani, M., 1996. Tectonique plio-quaternaire de la chaine tello-rifaine et de la mer d'Alboran; une zone complexe de convergence continent-continent. Bull. Soc. géol. Fr. 167 (1), 141–157.
Molin, P., Pazzaglia, F.J., Dramis, F., 2004. Geomorphic expression of active tectonics in a rapidly-deforming forearc, Sila massif, Calabria, southern Italy. Am. J. Sci. 304 (7), 559–589. https://doi.org/10.2475/ajs.304.7.559.
Méon, H., Tayech, B., 1986. Études palynologiques dans le Miocène du Cap Bon (Tunisie). Essai d'établissement d'écozones et de reconstitution paléogéographique. Geobios 19 (5), 601–626.
Molin, P., Fubelli, G., Nocentini, M., Sperini, S., Ignat, P., Grecu, F., Dramis, F., 2012. Interaction of mantle dynamics, crustal tectonics, and surface processes in the topography of the Romanian Carpathians: a geomorphological approach. Glob. Planet. Chang. 90, 58–72. https://doi.org/10.1016/j.gloplacha.2011.05.005.
Moulana, M.L., Hubert, A., Guendouz, M., El Ouahabi, M., Boutaleb, A., Boulvain, F., 2021. Contribution to the sedimentology of the Messinian carbonates of the Chelif Basin (Boukadir, Algeria). Geol. Belg. 24 (1–2) https://doi.org/10.20341/gb.2021.002.
Moulana, M.L., Hubert-Ferrari, A., Guendouz, M., Doutreloup, S., Robinet, S., Collignon, B., Ek, C., 2022. Karstic geomorphology of carbonate Ouarsenis Piedmont (Boukadir region, Chelif) in Algeria: the role of the Messinian Salinity Crisis. J. Afr. Earth Sci. 196, 104697 https://doi.org/10.1016/j.jafrearsci.2022.104697.
Mudd, S.M., Attal, M., Milodowski, D.T., Grieve, S.W., Valters, D.A., 2014. A statistical framework to quantify spatial variation in channel gradients using the integral method of channel profile analysis. J. Geophys. Res. Earth Surf. 119 (2), 138–152. https://doi.org/10.1002/2013JF002981.
Muhs, D.R., Budahn, J., Avila, A., Skipp, G., Freeman, J., Patterson, D., 2010. The role of African dust in the formation of Quaternary soils on Mallorca, Spain and implications for the genesis of Red Mediterranean soils. Quat. Sci. Rev. 29 (19–20), 2518–2543. https://doi.org/10.1016/j.quascirev.2010.04.013.
Naimi, M.N., Mansour, B., Cherif, A., 2020. First record of the Halimeda-rich beds from the Tessala–Beni Chougrane Messinian carbonate platform (Lower Chelif basin, NW Algeria). In: Conference: GeoConvention 2020. At: Calgary, Canada, 5 p.
Nehme, C., Farrant, A., Ballesteros, D., Todisco, D., Rodet, J., Sahy, D., Mouralis, D., 2020. Reconstructing fluvial incision rates based on palaeo-water tables in chalk karst networks along the Seine valley (Normandy, France). Earth Surf. Process. Landf. 45 (8), 1860–1876.
Neurdin-Trescartes, J., 1992. Le remplissage sédimentaire du bassin néogène du Chelif, modèle de référence de bassins intramontagneux. Thèse de Doctorat es Science, université de Pau et pays de l'Adour, France, 332 p.
Novello, A., Lebatard, A.E., Moussa, A., Barboni, D., Sylvestre, F., Bourles, D.L., A Paillès, C., Buchet, G., Decarreau, A., Duringer, P., Ghienne, J.-F., Maley, J., Mazur, J.-C., Roquin, C., Schuster, M., Vignaud, P., 2015. Diatom, phytolith, and pollen records from a 10Be/9Be dated lacustrine succession in the Chad basin: insight on the Miocene–Pliocene paleoenvironmental changes in Central Africa. Palaeogeogr. Palaeoclimatol. Palaeoecol. 430, 85–103. https://doi.org/10.1016/j.palaeo.2015.04.013.
Ouimet, W.B., Whipple, K.X., Granger, D.E., 2009. Beyond threshold hillslopes: channel adjustment to base-level fall in tectonically active mountain ranges. Geology 37 (7), 579–582. https://doi.org/10.1130/G30013A.1.
Ouyed, M., Meghraoui, M., Cisternas, A., Deschamps, A., Dorel, J., Frechet, J., Gaulon, R., Hatzfled, D., Philip, H., 1981. Seismotectonics of the El Asnam earthquake. Nature 292 (5818), 26–31. https://doi.org/10.1038/292026a0.
Pausata, F.S., Gaetani, M., Messori, G., Berg, A., de Souza, D.M., Sage, R.F., DeMenocal, P.B., 2020. The greening of the Sahara: past changes and future implications. One Earth 2 (3), 235–250. https://doi.org/10.1016/j.oneear.2020.03.002.
Pavano, F., 2013. Late Quaternary deformation of NE Sicily from relief and drainage system analysis. In: Rendiconti Online della Società Geologica Italiana, Vol. 29, pp. 134–137.
Pavano, F., Pazzaglia, F.J., Catalano, S., 2016. Knickpoints as geomorphic markers of active tectonics: a case study from northeastern Sicily (southern Italy). Lithosphere 8 (6), 633–648. https://doi.org/10.1130/L577.1.
Pérez-Peña, J.V., Azañón, J.M., Azor, A., 2009. CalHypso: an ArcGIS extension to calculate hypsometric curves and their statistical moments. Applications to drainage basin analysis in SE Spain. Comput. Geosci. 35 (6), 1214–1223. https://doi.org/10.1016/j.cageo.2008.06.006.
Perrodon, A., 1957. Publications du Service de la Carte géologique de l'Algérie, n.s., Bulletin, 12. Étude géologique des bassins néogènes sublittoraux de l'Algérie occidentale, 345 p.
Perron, J.T., Royden, L., 2013. An integral approach to bedrock river profile analysis. Earth Surf. Process. Landf. 38 (6), 570–576. https://doi.org/10.1002/esp.3302.
Perron, J.T., Dietrich, W.E., Kirchner, J.W., 2008. Controls on the spacing of first-order valleys. J. Geophys. Res. 113, F04016 https://doi.org/10.1029/2007JF000977.
Philip, H., Meghraoui, M., 1983. Structural analysis and interpretation of the surface deformations of the El Asnam earthquake of October 10, 1980. Tectonics 2 (1), 17–49. https://doi.org/10.1029/TC002i001p00017.
Reeve, T., 2021. Caves in the Chalk: a personal perspective from 50 years of observations. Cave Karst Sci. 48 (2), 3–18.
Riquelme, R., Martinod, J., Hérail, G., Darrozes, J., Charrier, R., 2003. A geomorphological approach to determining the Neogene to Recent tectonic deformation in the Coastal Cordillera of northern Chile (Atacama). Tectonophysics 361 (3-4), 255–275. https://doi.org/10.1016/S0040-1951(02)00649-2.
Rixhon, G., Bartz, M., El Ouahabi, M., Szemkus, N., Brückner, H., 2017. Contrasting terrace systems of the lower Moulouya river as indicator of crustal deformation in NE Morocco. J. Afr. Earth Sci. 126, 45–57. https://doi.org/10.1016/j.jafrearsci.2016.11.005.
Rodet, J., 1991. La craie, roche carbonatée poreuse et son karst. Karstologia 18 (1), 13–18.
Rodet, J., Laignel, B., Brocard, G., Dupuis, E., Massei, N., Viard, J.P., 2006. Contribution of a sedimentary study to the karstic evolution concept of a chalk cave of the Western Paris Basin (Normandy, France). Geol. Belg. 9 (3–4), 287–296.
Rohling, E.J., Cane, T.R., Cooke, S., Sprovieri, M., Bouloubassi, I., Emeis, K.C., Kemp, A. E.S., 2002. African monsoon variability during the previous interglacial maximum. Earth Planet. Sci. Lett. 202 (1), 61–75. https://doi.org/10.1016/s0012-821x(02)00775-6.
Rosenbaum, G., Lister, G.S., Duboz, C., 2002. Relative motions of Africa, Iberia and Europe during Alpine orogeny. Tectonophysics 359 (1–2), 117–129. DOI:1016/S0040-1951(02)00442-0.
Rouchy, J.M., Caruso, A., Pierre, C., Blanc-Valleron, M.M., Bassetti, M.A., 2007. The end of the Messinian salinity crisis: evidences from the Chelif Basin (Algeria).

Palaeogeogr. Palaeoclimatol. Palaeoecol. 254 (3–4), 386–417. https://doi.org/10.1016/j.palaeo.2007.06.015.
Roveri, M., Flecker, R., Krijgsman, W., Lofi, J., Lugli, S., Manzi, V., Sierro, F.J., Bertini, A., Camerlenghi, A., De Langj, G., Govers, R., Hilgen, F.J., Hübscher, C., Meijer, P.Th, Stoica, M., 2014. The Messinian Salinity Crisis: past and future of a great challenge for marine sciences. Mar. Geol. 352, 25–58. https://doi.org/10.1016/j.margeo.2014.02.002.
Royden, L., Perron, T., 2013. Solutions of the stream power equation and application to the evolution of river longitudinal profiles. J. Geophys. Res. Earth Surf. 118, 497–518. https://doi.org/10.1002/jgrf.20031.
Salzmann, U., Williams, M., Haywood, A.M., Johnson, A.L., Kender, S., Zalasiewicz, J., 2011. Climate and environment of a Pliocene warm world. Palaeogeogr. Palaeoclimatol. Palaeoecol. 309 (1–2), 1–8. https://doi.org/10.1016/j.palaeo.2011.05.044.
Schwanghart, W., Scherler, D., 2017. Bumps in river profiles: uncertainty assessment and smoothing using quantile regression techniques. Earth Surf. Dyn. 5 (4), 821–839. https://doi.org/10.5194/esurf-5-821-2017.
Scotti, V.N., Molin, P., Faccenna, C., Soligo, M., Casas-Sainz, A., 2014. The influence of surface and tectonic processes on landscape evolution of the Iberian Chain (Spain): quantitative geomorphological analysis and geochronology. Geomorphology 206, 37–57. https://doi.org/10.1016/j.geomorph.2013.09.017.
Shanahan, T.M., McKay, N.P., Hughen, K.A., Overpeck, J.T., Otto-Bliesner, B., Heil, C.W., King, J., Scholz, C.A., Peck, J., 2015. The time-transgressive termination of the African Humid Period. Nat. Geosci. 8 (2), 140–144. https://doi.org/10.1038/ngeo2329.
Sklar, L.S., Dietrich, W.E., 2004. A mechanistic model for river incision into bedrock by saltating bed load. Water Resour. Res. 40 (6).
Snyder, N.P., Whipple, K.X., Tucker, G.E., Merritts, D.J., 2000. Landscape response to tectonic forcing: digital elevation model analysis of stream profiles in the Mendocino triple junction region, northern California. GSA Bull. 112 (8), 1250–1263.
Stokes, M., Nash, D.J., Harvey, A.M., 2007. Calcrete 'fossilisation' of alluvial fans in SE Spain: the roles of groundwater, pedogenic processes and fan dynamics in calcrete development. Geomorphology 85 (1–2), 63–84. https://doi.org/10.1016/j.geomorph.2006.03.020.
Talling, P.J., Sowter, M.J., 1999. Drainage density on progressively tilted surfaces with different gradients, Wheeler Ridge, California. Earth Surf. Process. Landf. 24 (9), 809–824. https://doi.org/10.1002/(SICI)1096-9837(199908)24:9<809::AID-ESP13>3.0.CO;2-R.
Tavani, S., Corradetti, A., Sabbatino, M., Morsalnejad, D., Mazzoli, S., 2018. The Meso-Cenozoic fracture pattern of the Lurestan region, Iran: the role of rifting, convergence, and differential compaction in the development of pre-orogenic oblique fractures in the Zagros Belt. Tectonophysics 749, 104–119. https://doi.org/10.1016/j.tecto.2018.10.031.
Tayech, B., 1984. Etudes palynologiques dans le Néogène du Cap-Bon (Tunisie). These de Doctorat. Univ. Claude Bernard, Lyon I.
Tierney, J.E., Pausata, F.S., deMenocal, P.B., 2017. Rainfall regimes of the Green Sahara. Sci. Adv. 3 (1), e1601503 https://doi.org/10.1126/sciadv.1601503.
Trauth, M.H., Larrasoaña, J.C., Mudelsee, M., 2009. Trends, rhythms and events in Plio-Pleistocene African climate. Quat. Sci. Rev. 28 (5–6), 399–411. https://doi.org/10.1016/j.quascirev.2008.11.003.
Tucker, G.E., Bras, R.L., 1998. Hillslope processes, drainage density, and landscape morphology. Water Resour. Res. 34 (10), 2751–2764. https://doi.org/10.1029/98WR01474.
Vázquez, P., Menéndez, B., Denecker, M.F.C., Thomachot-Schneider, C., 2016. Comparison between petrophysical properties, durability and use of two limestones of the Paris region. Geol. Soc. Lond., Spec. Publ. 416, 203–216. https://doi.org/10.1144/SP416.15.
Wegmann, K.W., Pazzaglia, F.J., 2002. Holocene strath terraces, climate change, and active tectonics: the Clearwater River basin, Olympic Peninsula, Washington State. Geol. Soc. Am. Bull. 114 (6), 731–744. https://doi.org/10.1130/0016-7606(2002)114<0731:HSTCCA>2.0.CO;2.
Wells, D.L., Coppersmith, K.J., 1994. New empirical relationships among magnitude, rupture length, rupture width, rupture area, and surface displacement. Bull. Seismol. Soc. Am. 84 (4), 974–1002.
Whipple, K.X., 2004. Bedrock rivers and the geomorphology of active orogens. Annu. Rev. Earth Planet. Sci. 32, 151–185. https://doi.org/10.1146/annurev.earth.32.101802.120356.
Whittaker, A.C., 2012. How do landscapes record tectonics and climate? Lithosphere 4 (2), 160–164. https://doi.org/10.1130/RF.L003.1.
Willett, S.D., McCoy, S.W., Perron, J.T., Goren, L., Chen, C.Y., 2014. Dynamic reorganization of river basins. Science 343 (6175), 1248765. https://doi.org/10.1126/science.1248765.
Winterberg, S., Willett, S.D., 2019. Greater Alpine river network evolution, interpretations based on novel drainage analysis. Swiss J. Geosci. 112, 3–22. https://doi.org/10.1007/s00015-018-0332-5.
Wobus, C.W., Crosby, B.T., Whipple, K.X., 2006. Hanging valleys in fluvial systems: controls on occurrence and implications for landscape evolution. J. Geophys. Res. Earth Surf. 111 (F2) https://doi.org/10.1029/2005JF000406.
Wright, V.P., Tucker, M.E., 1991. Calcretes: an introduction. In: Wright, V.P., Tucker, M.E. (Eds.), Calcretes, IAS Reprint Series, Vol. 2. Blackwell Scientific Publications, Oxford, pp. 1–22.
Yaalon, D.H., 1987. Saharan dust and desert loess: effect on surrounding soils. J. Afr. Earth Sci. (1983) 6 (4), 569–571.
Yaalon, D.H., Ganor, E., 1973. The influence of dust on soils during the Quaternary. Soil Sci. 116 (3), 146–155.
Yelles-Chaouche, A., Boudiaf, A., Djellit, H., Bracene, R., 2006. La tectonique active de la région nord-algérienne. Compt. Rendus Geosci. 338 (1-2), 126–139. https://doi.org/10.1016/j.crte.2005.11.002.